INSTITUTE OF ASTRONOMY OF KHARKIV V. N. KARAZIN NATIONAL UNIVERSITY

KHARKIV 2009

Foreword

In 2008 Ukrainian astronomical community has commemorated 200 anniversary of astronomy in Kharkiv. This brochure is devoted to this anniversary and presents information on the Institute of Astronomy of Kharkiv V. N. Karazin National University. This is a compilation of inputs from different research groups and individuals of the Institute. The Report covers the staff and its activities including also a highlight reference list of publications. A short overview of the Institute history and the current status of its scientific activity are given.

ADDRESS:

Institute of Astronomy of Kharkiv V. N. Karazin National University,
35 Sumskaya St., 61022, Kharkiv, Ukraine

Director of Institute of Astronomy, Dr. Sci.,
Prof. Yuriy G. Shkuratov

Deputy Director Dr. Vladimir A. Psarev

Tel: +38 (057) 719 2882, 719 2883
Tel/FAX: +38 (057) 700-5349

e-mail: sky@astron.kharkov.ua

http://www.astron.kharkov.ua

CONTENT

Page

1. Brief History……4

2. Scientific Council of the Institute……12

3. Institute Staff……12

4. Selected Research Activities……14

4.1. Lunar Studies, *Yu. G. Shkuratov, V. V. Korokhin, V. G. Kaydash, N. N. Opanasenko,Yu. I. Velikodsky*……14

4.2. Asteroids and Comets, *D. F. Lupishko, I. N. Belskaya, Yu. N. Krugliy, V. G. Shevchenko, F. P. Velichko* ……19

4.3. Martian UV Clouds Observed by Hubble Space Telescope in Polarized Light in 2003, *Yu. G. Shkuratov, V. G. Kaydash* ……24

4.4. Jupiter's Atmosphere, *O. S. Shalygina, V. V. Korokhin, E. V. Shalygin, G. P. Marchenko, Yu. I. Velikodsky, L. V. Starukhina, O. M. Starodubtseva, L. A. Akimov*……27

4.5. Light Scattering by Particles and Particulate Surfaces, *Yu. G. Shkuratov, E. S. Zubko, V. A. Psarev, A. A. Ovcharenko* ……30

4.6. Implanted Gases on Atmosphereless Celestial Bodies, *L. V. Starukhina* ……32

4.7. Solar Studies, *L. A. Akimov, I. L. Belkina, V. V. Korokhin, G. P. Marchenko*……35

4.8. Gravitational lenses, *V. N. Dudinov, V. G. Vakulik, V. S. Tsvetkova, V. V. Konichek, A. P. Zheleznyak*……37

4.9. Globular Cluster M15: New Variable Stars, *A. P. Zheleznyak*……41

4.10. The Kharkiv's XC1 catalogue of positions and proper motions of faint stars around extragalactic ICRF sources, *P. N. Fedorov, A. A. Myznikov* ……43

4.11. Absolute proper motions of 280 millions stars from 2MASS and USNOA2.0 data, *P. N. Fedorov, A. A. Myznikov, V. S. Akhmetov*……45

5. Other Activities……47

6. Selected papers ……49

1. Brief History

The Research Institute of Astronomy of V. N. Karazin National University in Kharkiv was founded in 2002 on the basis of the Astronomical Observatory of the University, one of the eldest observatories in Ukraine. Our Observatory was founded by Prof. G. V. Levitskiy (1852–1917) in 1883 (see Fig. 1), though astronomical studies at Kharkiv University began in 1808 when a laboratory equipped with astronomical instruments was opened.

Since the foundation many famous scientists worked at the Observatory. Prof. L. O. Struve (1858-1920) was a founder of Kharkiv astrometry and stellar astronomy. The famous astrophysicist Academician V. G. Fesenkov (1889-1972) started planetary studies at the Observatory. Prof. B. P. Gerasimovich (1889-1937) originated here theoretical astrophysics. Later, in 1930's, he was the Director of Pulkovo Observatory (Russia). American astronomer Otto Struve (1897-1963) started his scientific career in Kharkiv University; as is well-known, later he headed a number of American astronomical institutions and was the President of the International Astronomical Union. Famous scientist Academician N. P. Barabashov (1894–1971) began in 1918 his systematic studies of the Moon and planets in Kharkiv (see Fig. 2). This gave the origin of many recent planetary investigations at our Institute. N. P. Barabashov discovered the lunar backscatter effect, the analogues of which are now deeply studied in different fields of physics.

During almost 110 years astrometric measurements continued giving significant inputs for several fundamental catalogues. In 1935 a spectroheliograph, the first instrument of such a kind in the USSR, was designed and constructed. Then the monitoring of Solar activity was organized giving the origin of studies in Solar physics at the Observatory. In 1933 the Kharkiv Time Service as a component of the International Time Service began its daily routine work. Many other investigations were carried out, however, the main results of Kharkiv astronomers were obtained in the field of planetary science. Information about the Moon's surface, Martian surface, atmosphere and dust storms, studies of the photometric properties of Venus, Jupiter, and Saturn obtained by researchers of our Observatory in 1950-70’s ensured, in particular, greater efficiency of the first Soviet planetary space missions. Intensive work related to the design of spacecraft astronavigation systems was performed in 1967–1988. Recent planetary studies in the Institute are related to telescope photometric and polarimetric observations

of asteroids, comets, and the Moon. Kharkiv astronomers analyze results of space missions to the Moon (Clementine, Lunar Prospector, and Smart-1), Mars (Mars Global Surveyor), Venus (Pioneer-Venus, Magellan, and Venera 13-16), and Phobos (Phobos mission). Since the end of the 60's successive efforts were undertaken to develop image-processing algorithms for high-resolution imaging with ground-based optical telescopes. During last time important studies on laboratory, computer, and theoretical modeling of light scattering by regolith-like surfaces were carried out.

Figure 1. Grigoriy V. Levitsky (1852-1917), the founder of Kharkov Astronomical Observatory

Figure 2. Nikolay P. Barabashov (1894-1971), the founder of planetary schools of thought in Kharkiv University

Figure 3. Telescope AZT-8 of Institute of astronomy

Figure 4. The dome of telescope Mertz and building of Kharkov University

Instruments

The main instruments of the Institute are the 0.7-m reflector AZT-8 (see Fig. 3), the spectro-heliograph, and the solar telescope AFR-2. For educational purposes the 20 cm reflector AZT-7, Repsold meridian circle, and the 20 cm Zeiss refractor are used. The coherent-optical device, allowing one to produce Fourier transformation of images and to measure scattering properties of objects with complicated structure, was registered as the National Property of Ukraine. At present time this device is used for laboratory measurements of the backscattering effect of particulate surfaces at very small phase angle (starting from 0.002°). Our observers have had opportunities to work with powerful instruments at other observatories including the NASA/ESA Hubble Space Telescope (HST), the 8.2-meter telescope at the Paranal Observatory, and the 6-meter BTA telescope in Russia (SAO RAS).

Institute Structure

The Institute has two territories. The first one is at the center of Kharkiv, near the National University building (see Fig. 4). The second one, Chuguev Observational Station, is located at 75 km to south-east from Kharkiv. In the last years the scientific staff of the Institute and the chair of astronomy comprises 35 researchers (4 teachers) in permanent positions including 7 Doctors of Science (Professors) and 18 Candidates of Science (PhDs). The supporting staff is 25 persons. The researchers are organized in four departments and one laboratory (Fig. 5-10):

- Department of Physics of Asteroids and Comets (headed by Prof. D. F. Lupishko);
- Department of Remote Sensing of Planets (headed by Prof. Yu. G. Shkuratov);
- Department of Astrophysics (headed by Dr. Sci. V. N. Dudinov);
- Department of Planetary and Solar Physics (headed by Dr. V. V. Korokhin);
- Laboratory of Astrometry (headed by Dr. P. N. Fedorov).

The teachers are organized in Chair of Astronomy headed by Dr. A. M. Gretskiy.

Our Institute has a museum and a library: above 50.000 of the principal astronomical and scientific periodicals and books, including folios from private V. N. Karazin and L. O. Struve libraries. The museum has instruments delivered to Kharkiv in 1808 by J. S. Huth who was the first astronomer in Kharkiv University.

Figure 5. Department of Astrophysics. From left to right: Alexander P. Zleleznyak, Igor E. Sinel'nikov, Alexey Sergeyev, Vladimir N. Dudinov (Head of Dep), Alexey E. Kochetov, Victor G. Vakulik, Elena Y. Bannikova, Victoriya S. Tsvetkova, Gleb Smirnov, Vladimir V. Konichek

Figure 6. Department of Remote sensing of planets. From left to right: Vladimir A. Psarev, Sergey Y. Gerasimenko, Dmitriy G. Stankevich, Nikolay V. Opanasenko, Larisa G. Istomina, Dmitriy V. Petrov, Larisa V. Starukhina, Tatyana I. Suchkova, Sergey Y. Bondarenko, Yuriy G. Shkuratov (Head of Dep.), Andrey A. Ovcharenko

Figure 7. Department of Physics of Asteroids and Comets. From left to right, first line: Nikolay N. Kiselev, Irina N. Belskaya, Dmitriy F. Lupishko (Head of Dep.), and second line: Fedor P. Velichko, Vasiliy G. Shevchenko, Vasiliy G. Chorniy, Yuriy N. Krugliy

Figure 8. Department of Planetary and Solar physics. From left to right: Oksana Shalygina, Yuriy I. Velikodsky, Victor V. Korokhin, Evgeniy Shalygin, Inna L. Belkina, Leonid A. Akimov

Figure 9. Laboratory of Astrometry. From left to right: Nikolay S. Olifer, Vladimir A. Zakhozhay, Lidiya G. Opanasenko, Petre N. Fedorov, Vitaliy S. Filonenko, Andrey A. Myznikov

Figure 10. Chair of Astronomy of Kharkiv University. From left to right, first line: Andrey M.Getskiy (head of chair), Nikolay N. Evsukov, Valentina I. Latsko, Yuriy V. Alexandrov, and Yuriy G. Shkuratov, second line: Petre N. Fedorov, Vladimir A. Zakhozhay, Vasiliy G. Shevchenko, and Dmitriy G. Stankevich

Scientific Activity

The basic studies of the Institute are:

- composition and structure characteristics of the lunar and planetary surfaces and atmospheres, which are estimated with combining ground-based telescope and spacecraft observation data;
- physical properties of minor planets and comets with applications to the impact hazard problem;
- experimental and theoretical modeling of light scattering by dust particles and particulate surfaces;
- photometric monitoring of brightness variations in gravitational lens systems and investigation of gravitational lensing phenomena;
- solar activity in the chromosphere with solar monitoring;
- meridian and positional astrometry using photoelectric and CCD-methods.

Since the foundation Kharkiv astronomers have published near 3200 papers. At present time the number of peer-reviewed publications including international journals (like Icarus, Astronomy and Astrophysics) and abstracts is about 100 each year.

Educational Activity

Scientific researches and education in Kharkiv National University are closely associated. About ten astronomy students graduate every year. During six post-war decades about 400 qualified astronomers graduated from Kharkiv University. Unfortunately, most of the students are not going to make a career in astronomy, nevertheless, about 100 of our students have been awarded the Candidate (PhD) degree, and 25 persons were awarded the Dr. Sci. degree.

Community Recognition

Several astronomers of Kharkiv National University are members of International Astronomical Union, European Astronomical Society, and American Astronomical Society. Our scientific achievements are highly appreciated: 32 objects of the Solar system are named in honor of Kharkiv astronomers. Four laureates of the Ukrainian State Prize and four laureates of the Prizes of National Academy of Sciences of Ukraine are working at the Institute. Kharkiv astronomers are constant reviewers of several international journals, like

Icarus, Journal Geophysical Research (Planets), Astrophysical Journal, Planetary and Space Science, and others.

International Cooperation

Astronomers of Kharkiv National University work in close co-operation with their colleagues from astronomical institutions of Ukraine, Russia, Uzbekistan, and other countries of the former USSR, and USA, France, Germany, Italy, Finland, Czech Republic, Japan, Spain, Argentina, Bulgaria, Sweden, and Poland.

Prof. Yuriy G. Shkuratov, Editor.

Kharkiv 2009

2. Scientific Council of the Institute

Prof. Y. G. Shkuratov (chairman), Dr. L. A. Akimov, Prof. Y. V. Alexandrov, Dr. I. N. Belskaya (secretary), Dr. V. N. Dudinov, Dr. P. N. Fedorov, Dr. A. M. Gretskiy, Dr. V. G. Kaydash, Dr. V. V. Korokhin, Dr. Y. N. Krugliy, Prof. D. F. Lupishko, Dr. A. A. Minakov (Radioastronomy Institute), Dr. V. A. Psarev (vice chairman), Dr. D. G. Stankevich, Dr. A. A. Ovcharenko, V. G. Vakulik, Dr. Y. I. Velikodskiy, N. A. Vorob'eva.

3. Institute Staff

The staff includes scientists with permanent positions.

Department "Physics of Asteroids and comets"
Dmitry F. Lupishko, Prof., Dr. Sci., Head of Dept.
Irina N. Belskaya, Dr. Sci., Leading Researcher
Fedor P. Velichko, PhD., Leading Researcher
Yuriy N. Krugliy, PhD., Senior Researcher
Vasiliy G. Chorniy, Researcher
Vasiliy G. Shevchenko, PhD., Senior Researcher (combine jobs)

Department "Remote Sensing of Planets"
Yuriy G. Shkuratov, Prof., Dr. Sc., Head of Dept., Director
Vadim G. Kaydash, PhD., Senior Researcher
Larissa V. Starukhina, PhD., Leading Researcher
Dmitriy V. Petrov, PhD., PhD., Senior Researcher
Nikolay V. Opanasenko, PhD., Senior Researcher
Andrey A. Ovcharenko, PhD., Senior Researcher, Head of Chuguev Observ. Station
Evgenij S. Zubko, PhD., Senior Researcher
Sergey Y. Bondarenko., Researcher

Department "Astrophysics"
Vladimir N. Dudinov, Dr.Sc., Head of Dept.
Victor G. Vakulik, Senior Researcher
Alexander P. Zheleznyak, PhD., Senior Researcher
Vladimir V. Konichek, Researcher

Igor E. Sinelnikov, Researcher
Alexey E. Kochetov, Researcher
Gleb V. Smirnov, Researcher
Oleg B. Zaslavsky, Dr. Sci., Senior Researcher

Department "Planetary and solar physics"
Viktor V. Korokhin, PhD, Head of Dept.
Leonid A. Akimov, Dr Sc., Leading Researcher
Yuriy I. Velikodskiy, PhD., Senior Researcher
Evgeniy V. Shalygin, Junior Researcher
Oksana S. Shalygina, Junior Researcher
Inna L. Belkina, Senior Researcher
Gennadiy P. Marchenko, Researcher

Laboratory "Astrometry and Stellar Astronomy"
Peter N. Fedorov, PhD, Head of Laboratory
Vladimir A. Psarev, PhD. Deputy Director of the Institute
Vitaliy S. Filonenko, Researcher
Nikolay S. Olifer, Researcher
Angela I. Pisarenko, PhD., Researcher

Chair of Astronomy
Yuriy V. Alexandrov, PhD., Professor, Head of the Chair till 2004
Andrey M. Gretskiy, PhD., Professor assistant, Head of the Chair since 2004
Dmitriy G. Stankevich, PhD., Professor assistant
Vasiliy G. Shevchenko, PhD., Professor assistant
Vladimir A. Zakhozhay, Dr. Sci., Professor

4. Selected Research Activities

4.1. Lunar Studies

Yu. G. Shkuratov, V. G. Kaydash, V. V. Korokhin, N. N. Opanasenko, Yu. I. Velikodsky

The main goal of our optical investigations of the Moon is the prediction and mapping of chemical and mineral composition parameters of the lunar surface and its structure properties. For this purpose we use Clementine, Lunar Prospector, and Smart-1 data as well as data of laboratory measurements of lunar samples (LSCC data). Our studies also are devoted to photometric and polarimetric studies of the Moon with telescopes. We consider below several examples.

Phase-angle-ratio technique

The brightness of the lunar surface depends on the phase angle. This dependence, referred as the phase function, is controlled by the regolith structure at wide range of spatial scales. The phase function can be approximated with an exponential curve. Anomalies in the phase function (e.g., much variations of its steepness or exponent) indicate anomalies in the regolith structure. We use a series of 52 images of a vicinity of the Apollo-15 landing site taken with Clementine UVVIS camera in orbit 299 to retrieve information about regional distribution of the parameter characterizing the steepness that is the exponent. The spacecraft moved from South to North almost through the local zenith. The phase angle changed in the range of 26° – 55° through the series. The image taken almost from the zenith is shown in Fig. 11 a. The image resolution is about 200 m. The map of the phase function steepness is shown in Fig. 11 b. A contrasting shadow-like pattern of mountains (Apennines) and a channel (Rima Hadley) does not reflect real variations of the photometric function parameters and should be disregarded in the analysis. These strong variations are caused by relatively steep surface slopes which were not taken into account when we calculated the observation geometry. One can see several distinctive diffuse features on the flat mare surface. The most pronounced feature is a diffuse crater halo shown with the arrow B and C in Fig. 11 b. A small dark spot (right arrow A in Fig. 11 b) is not associated with any fresh crater but exactly coincides with the Apollo 15 landing site. The anomaly is related to damages of the regolith structure around the landing site; it is probably caused with the lander jets. In addition, using another data, the anomalies were found for fresh lunar craters and some volcanic edifices. In the latter case the anomalies are due to pyroclastic deposits.

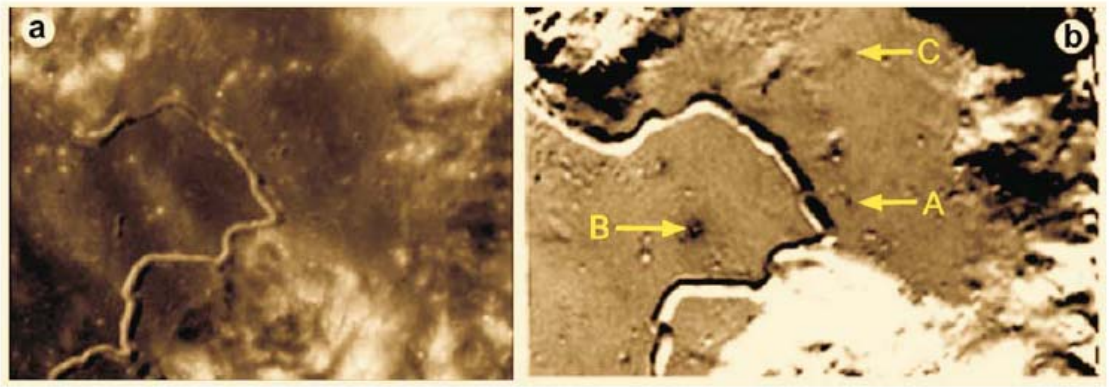

Figure 11. Image of Apollo-15 landing region (a). Rima Hadley is clearly seen. Brighter shades denote higher steepness of brightness phase curve (b). Arrows A, B, and C) show the landing site and young craters.

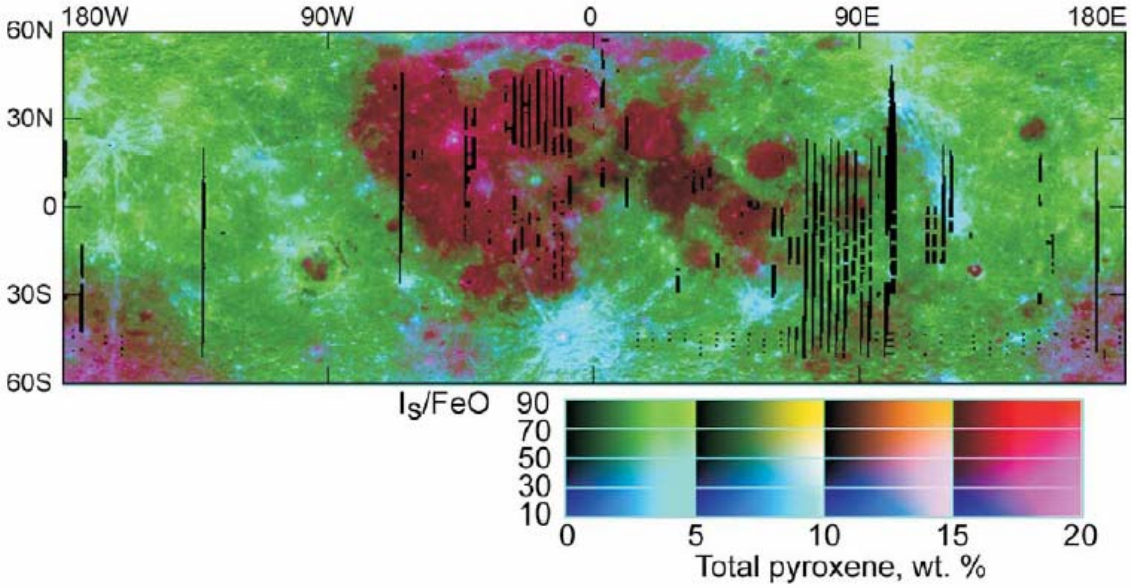

Figure 12. Two-parametric map of the maturity degree and total pyroxene abundance of the lunar surface.

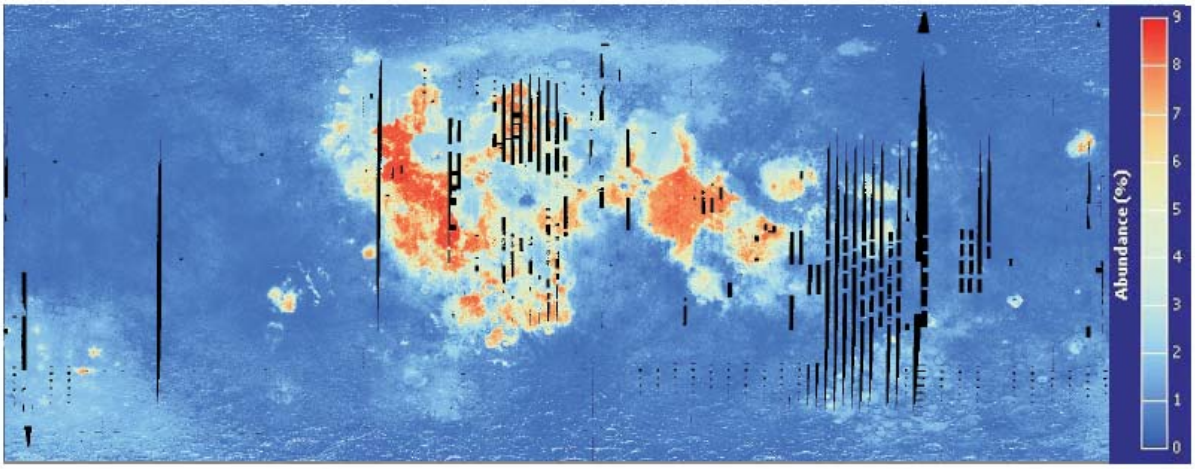

Figure 13. Distribution of TiO_2 over the lunar surface mapped using Clementine mosaics with application of artificial neural networks to analysis of correlations between optical and chemical characteristic of lunar samples (LSCC data)

Mapping of surface composition

A new approach for remote sensing determination of the lunar surface composition has been proposed in our Institute. The technique uses Clementine UVVIS data and results of spectral and chemical/mineral studies of lunar samples by the Lunar Soil Characterization Consortium [Pieters et al. Icarus 2002, 155, 285]. The main rock-forming oxides (FeO, TiO_2, Al_2O_3), minerals (pyroxene, plagioclase), and maturity degree (I_s/FeO) were mapped with 1 km resolution. To map chemical/mineral parameters of the lunar surface we use images acquired in the following four Clementine UVVIS camera spectral bands: 415, 750, 900, and 1000 nm. The correlations between the linear combinations of albedo measured in the mentioned spectral bands and chemical/mineral characteristics for lunar 52 samples allow prognosis lunar maps of the characteristics. An example of applying such a technique is presented in Fig. 12 that is a lunar two-parameter map of the maturity degree, I_s/FeO, and total pyroxen content in lunar soil. The parameter I_s/FeO is the ratio of ferromagnetic resonance intensity I_s (which is proportional to metallic iron content) to the total Fe content. It is closely related to the age (exposition time) of the lunar surface. Our analysis shows that the regoliths of morphologically young craters are characterized with low degree of maturity and high content of pyroxene. Small areas with anomalous high maturity degree are found. They are mainly located at the center of the lunar nearside and associated with so-called dark mantle deposits.

We also have suggested a technique to determine the chemical and mineral composition of the lunar surface using artificial neural networks (ANN). We demonstrate this powerful non-linear approach for prognosis of TiO_2 abundance (see Fig. 13) using the Clementine UVVIS mosaics and Lunar Soil Characterization Consortium data. The ANN technique allows one to study correlations between spectral characteristics of lunar soils and composition parameters without any restrictions on the character of these correlations.

The results obtained could be useful for the strategy of analysing lunar data that will be acquired in incoming lunar missions especially in case of the Chandrayaan-1 and Lunar Reconnaissance Orbiter missions.

Polarimetric studies

Polarimetric investigations of the Moon have a long history. They are not being actively pursued. One reason is that at large phase angles there is an inverse correlation between albedo *A* and polarization degree P of light scattered by the lunar surface. This effect is often called Umov's law. The correlation is approximately linear on a log-log

scale: log$P$ + $a$log$A$ = b, where a and b are constants. The correlation coefficient is up to 0.95. Because of this correlation, mapping polarization degree often is considered as non-informative for remote sensing of the lunar surface.

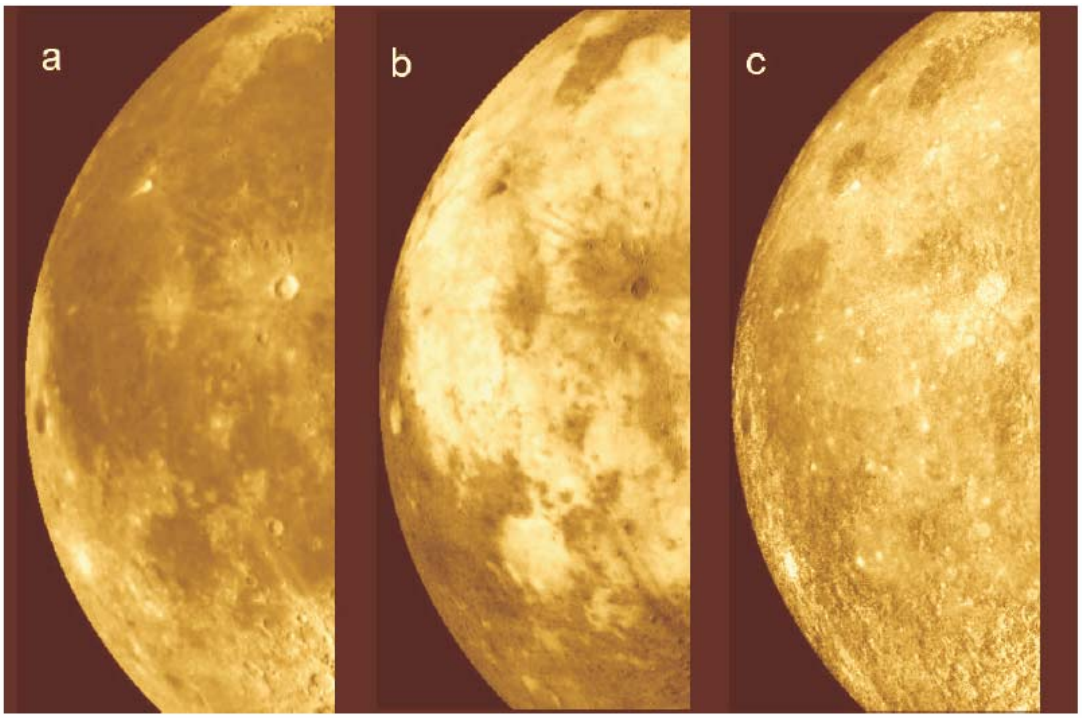

Figure 14. Image of west portion of the Moon with compensation of longitude and latitude dependence of brightness – (a), distribution of linear polarization degree at phase angle 88° – (b), distribution of the parameter b = log AP^{a}_{max} – (c)

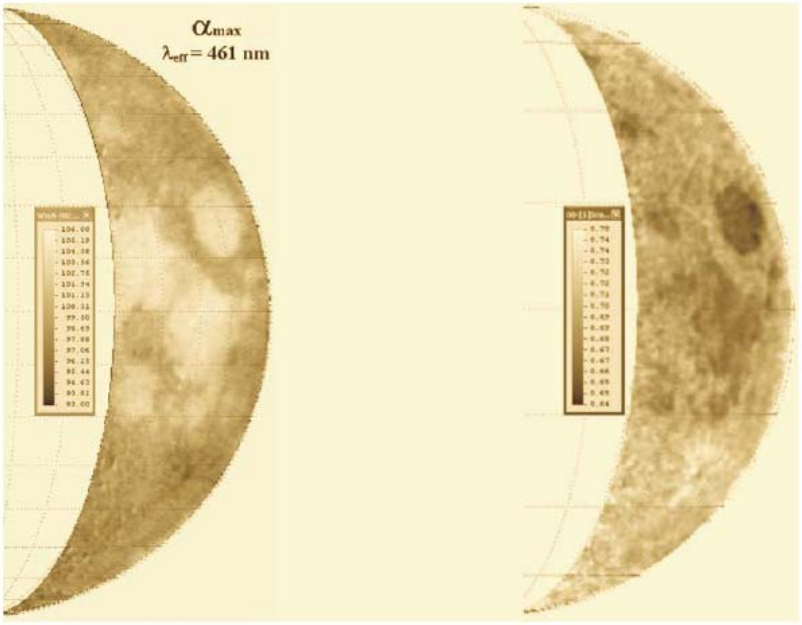

Figure 15. Mapping the position of the maximum of positive polarization $\alpha_{max}(\lambda_{eff}$=461 nm). East portion of the Moon

Figure 16. Mapping the ratio P_{max}(670 nm)/P_{max}(460 nm). East portion of the lunar nearside

First attempts to acquire further information from polarization have been undertaken in Kharkiv observatory by quantifying the deviation of the polarization from the regression line of the albedo correlation. To characterize the deviations, the parameter $(P_{max})^a A$ has been proposed. It has been shown that the parameter bears significant information on the characteristic size and microporosity of the lunar regolith. Analysis of the images of the distribution of $(P_{max})^a A$ shows the following (see Fig. 14): (1) rayed young craters including the Aristarchus crater have increased values of the parameter, perhaps because of the immature character of the regolith (coarse grains); and (2) regions characterized by decreased values of $(P_{max})^a A$, e.g., Aristarchus Plateau and Marius Hills area that are regions of volcanism that could be accompanied by ash deposits containing fine (dust) particles. Figure 14 a shows an image of the lunar albedo for the western portion of the lunar nearside. The image has been obtained at the wavelength 0.43 μm. The brightness trend from the lunar limb to the terminator has been compensated. Figure 14 b shows the distribution of the degree of linear polarization that is very similar to an albedo negative of Figure 14 a, owing to that there is the inverse correlation between albedo and polarization degree. Figure 14 c is the image demonstrating the distribution of the parameter $(P_{max})^a A$. Laboratory measurements of lunar samples and size-particle separates of terrestrial glasses have shown that the variations of this parameter are closely correlated with the particle size. Young craters are clearly visible in Fig. 14 c indicating their coarse regolith particles.

Polarimetric observations of the lunar surface with an imaging CCD–polarimeter were carried out at 23 phase angles, from 8° to 123°. The values of positive polarization degree maximum P_{max} and its phase angle α_{max} in two spectral bands, λ_{eff} = 461 nm and λ_{eff} = 669 nm, for the east portion of the lunar nearside have been mapped. Examples of mapping the parameters of maximum polarization: (a) α_{max} at λ_{eff} = 461 nm and (b) Cp_{max} = P_{max}(669 nm) / P_{max}(461 nm) are shown in Fig. 15. As can be seen the parameter α_{max} and albedo of the lunar surface anticorrelate with each other. The correlation diagram "Cp_{max} – albedo" shows that there is an anticorrelation for mares and direct correlation for highlands. The histogram of P_{max} distribution over the portion of the lunar disk has a distinct maximum at P_{max} = 7.3 % for λ_{eff} = 461 nm and that at P_{max} = 5.25 % for λ_{eff} = 669 nm. The range of P_{max} variations is 4.0 ... 21.0 % for λ_{eff} = 461 nm and 3.0 ... 15.0 % for λ_{eff} = 669 nm. The histogram of α_{max} distribution is distinctly bimodal with the first peak at α = 99.7° (highlands), and the second one at α = 104.1° (mares) for λ_{eff} = 461 nm. For λ_{eff} = 669 nm we have α = 96.8° and α = 101.2°, respectively. The histogram is narrower in blue

light, 94.0° ... 106.0°, as compared to that in red light (90.0° ... 105.0°). The maximum of polarization occurs at larger phase angles in the blue band.

4.2. Asteroids, Comets and Transneptunian Objects

D. F. Lupishko, I. N. Belskaya, Yu. N. Krugly, V. G. Shevchenko, F. P. Velichko

For the last years our principal research were directed to study physical properties of main-belt asteroids, near-Earth asteroids, comets, and Transneptunian objects on the base of their photometric and polarimetric obsevations. The main research programs include:

- Asteroid shapes and rotation parameters;
- Searching for and study of binary systems among near-Earth and main-belt asteroids;
- Opposition effect, magnitude-phase dependences and other optical properties of asteroids;
- Light scattering and physical properties of comet dust;
- Physical properties of Transneptunian objects.

Photometry of main-belt and near-Earth asteroids

Photometric observations were curried out at the Institute Observation Station (in 75 km from Kharkiv city) with the 0.7 m reflector AZT-8 equipped with photoelectric photometer-polarimeter and CCD cameras ST-6, IMG 1024 and IMG 47-10 (Finger Lake Instrumentation). A portion of photometric observations was curried out at the Crimean Astrophysical Observatory with the 1 m reflector (Simeiz) and CCD cameras ST-6 and Apogee Alta. During 370 nights the photometric observations of 101 asteroids (including 34 NEAs and 3 Mars-crossers) were carried out and their lightcurves and color indexes were obtained and used for study of asteroid shapes, sizes, rotation parameters, optical properties of their surfaces, for discovery and study binary systems, etc. Besides, the CCD follow-up observations of the several newly discovered near-Earth asteroids were carried out and processing (Velichko F., Shevchenko V., Krugly Yu., Chiorny V.). As a result of this program the rotation periods of 40 asteroids, the UBVRI-color indexes, compositional types and the estimates of absolute magnitudes and sizes of several tens asteroids were obtained. Our observations of 1682 Apollo at Simeiz Observatory in November 2005 were carried out in frame of International observation network managed by M. Kaasalainen

(University of Helsinki). Analysis of available Apollo's data has showed a change in the rotation rate of the asteroid, which is best explained by the YORP effect. The change is fairly large and clearly visible in photometric lightcurves, amounting to one extra rotation cycle in just 40 years even though Apollo's size is well over one kilometer. This confirms the prediction that the YORP effect plays significant role in the dynamical evolution of asteroids (Krugly Yu.).

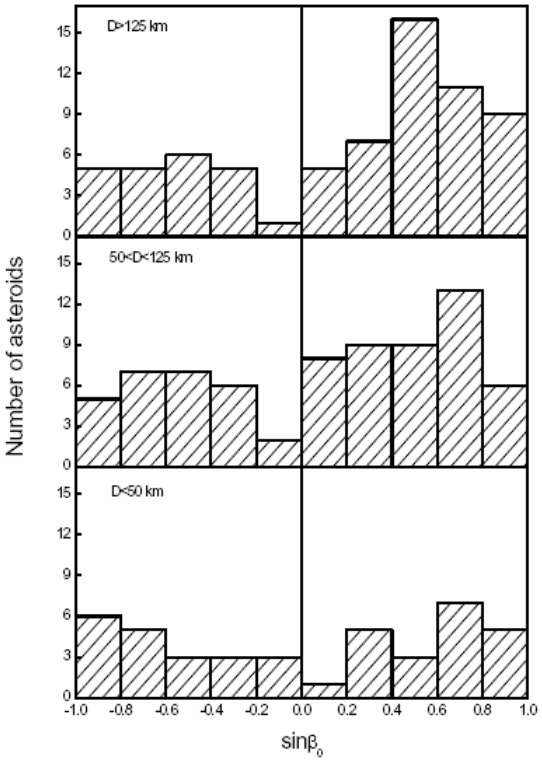

Figure 17. Distribution of ecliptic latitudes of asteroid poles for different range of asteroid diameters (sinβ0>0 – prograde rotation, sinβ0<0 – retrograde).

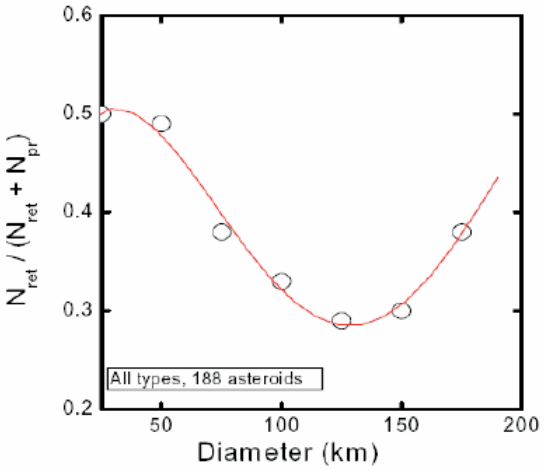

Figure 18. Dependence of a portion of asteroids with retrograde rotation on their diameters.

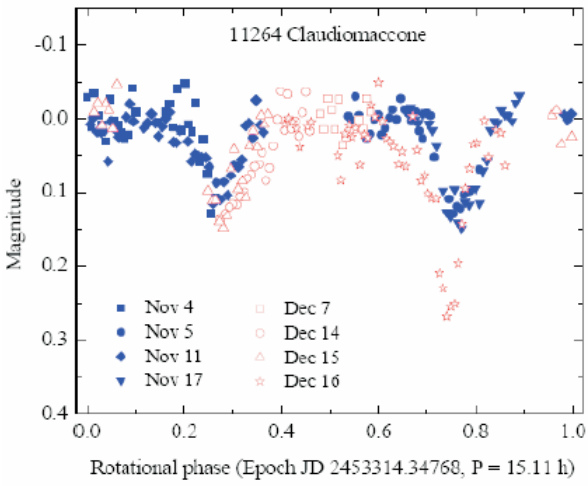

Figure 19. Composite lightcurve of the long-period component of binary asteroid11264 Claudiomaccone

The method of inverse task solution for the determination of asteroid pole coordinates, sidereal periods of rotation, senses of rotation, and ratios of semi-axis of their figures was improved. Using this method the foregoing parameters for 55 asteroids (including 11 near-Earth ones) were determined. Analyzing these and all available data (about 200 asteroids) an anisotropy in the distribution of ecliptic latitudes of asteroid poles with maximum at near middle latitudes ($\beta_0 = 40 \pm 4°$) was confirmed. For the first time it was shown that the anisotropy takes place only for objects with prograde rotation (see Fig. 17, $\sin\beta_0 > 0$). Moreover the degree of anisotropy increases with asteroid diameters. The ratio of asteroids with prograde and retrograde rotations increases with their diameters from 1:1 among the small asteroids (D < 50 km) to 1.5:1 among the intermediate (50<D<125 km) and to 2:1 among the large ones (D > 125 km). These conclusions have a cosmogonic character and are evidence of the intensive collision evolution in asteroid belt (Shevchenko V., Lupishko D.).

The clear minimum at D = 125 km in the dependence of a portion of asteroids with the retrograde rotation on their diameter was confirmed using the sample of data 2.5 times larger than it was analyzed before (Fig. 18). As is well known, the similar minimum at this diameter also exists in the dependences of rotation rates and lightcurve amplitudes on asteroid diameters. New and more complete data show that the depth of the minimum for M-asteroids is much greater than for C and S-types and probably correlates with asteroid density increasing from less dense C-type to S and to most dense M-type. Thus, asteroid diameter of 125 km is a cosmogonic peculiarity, and its quantitative explanation can give valuable information on dynamical evolution in asteroid belt (Lupishko D.).

Searching for and study of the binary systems among asteroids

Our photometric CCD-observations of the small main-belt asteroid 11264 Claudiomaccone, which were carried out with the 0.7 m telescope at Chuguev Observation Station in November 2004 and the 1-m telescope at Simeiz Observatory in Dec. 2004, have shown the presence of two different periods in asteroid brightness variations. A short period of 3.1872 ± 0.0006 h and long one of 15.11 ± 0.01 h were determined. The analysis of lightcurves allowed us to suppose that asteroid 11264 Claudiomaccone is an asynchronous binary system in the main belt (Fig. 19). The parameters of the system are estimated to be as follows: the ratio of the secondary to primary diameters is ≥ 0.31, the ratio of the orbital radius to the primary's diameter is

about 1.5 and a bulk density of the primary body is $\rho_p \geq 1.2$ g/cm^3 (Krugly Yu., Lupishko D., Shevchenko V., Velichko F.).

Since 2005 we take part in the International observational program “Photometric Survey for Asynchronous Binary Asteroids” established by P. Pravec at Ondrejov Observatory in the end of 2004. The project is aimed for search and investigation of the binaries between NEAs and small main-belt asteroids with D<15 km. In the frame of this program we observed more than 20 asteroids among them 10 ones were revealed as binaries (Krugly Yu., Chiorny V., Shevchenko V.).

Magnitude-phase dependences and other optical properties of asteroids

The magnitude-phase dependences down to small phase angles were measured (mainly in the V band) for more than 50 asteroids of diverse surface composition. The observations let us to search for possible correlation of phase curve parameters and asteroid surface properties. A strong correlation has been found between phase coefficients and albedos, which can be used for asteroid albedo estimations. At phase angles > 5° up to 25° the phase slopes increase linearly as albedo decreases assuming dominating contribution of the shadow-hiding effect in this phase angle range and a similarity of surface texture of the studied asteroids. At smaller phase angle range (0.3 – 5°) we found non-monotonic dependence of the phase slopes on asteroid albedo. The maximum value of the phase slope defined as I(0.3°)/I(5°) is observed for moderate albedo asteroids decreasing both for dark and high albedo surfaces. It can be explained by an increasing influence of the coherent-backscatter mechanism at small phase angles which is more prominent for high-albedo surfaces. Low albedo asteroids are found to have the smallest amplitude of the opposition effect and its largest dispersion as compared to other asteroid types. A special program to study brightness opposition effect for low albedo asteroids has been carried out last years. We measured phase curves down to extremely small phase angles 0.1 – 0.3° for about 15 low albedo asteroids and found 3 asteroids for which the brightness behavior in the range of opposition effect is almost linear (190 Ismene, 419 Aurelia, 1021 Flammario). These asteroids are assumed to have the darkest surfaces where the shadow-hiding mechanism alone forms brightness behaviour near opposition. Other low albedo asteroids measured so far show typical opposition effect with amplitude about 0.1-0.2 mag relative to the extrapolation of the linear part of phase curve toward opposition (Shevchenko V. G., Belskaya I. N., Chiorny V. G., Krugly Yu. N.).

For asteroids 419 Aurelia and 1021 Flammario with the smallest opposition effect value we carried out polarimetric observations to measure polarization phase functions. It was found that both asteroids are characterized by unusually shallow negative branch with small inversion angle atypical for other low albedo asteroids (Belskaya I. N.).

Photometry and polarimetry of comets

Photometric and polarimetric observations of the dynamically new comet C/2002 T7 (LINEAR) and periodical comets 153P/Ikeya-Zhang, 2P/Encke and 73P/Schwassmann-Wachmann 3 are carried out using the 0.7 m reflector of our Institute and 1.25 m and 2.6 m reflectors of Crimean Astrophysical Observatory (Ukraine) with UBVRI-polarimeter. It was shown that a number of gas-rich comets have low polarization degree at large phase angles and blue color mainly due to low spectral and spatial resolution of the measurements. The dust-rich comet 153P/Ikeya-Zhang in continuum filter GC (λ 5652/57 angstrem) has shown low polarization degree because of that the comet spectrum has an unidentified emission line overlapping the GC-band (Velichko F., Velichko S.). The nucleus C of the gaseous comet 73P/Schwassmann-Wachmann 3 shows phase dependence of polarization at $\alpha = 48 \div 95°$ in red continuum RC (λ 6840/90 angstrem). This dependence is close to the average one of dusty comets, but far than that for so-called gaseous comets (Velichko F., Kiselev N., Velichko S.). Otherwise, polarimetry of the gaseous comet 2P/Encke shows that dust polarization may be as high as in the so-called dusty comets. Thus the dichotomy in polarization of dust-rich and gas-rich comets is probably an artifact caused by the gas emissiom transmitted by cometary “continuum” filters (Kiselev N.).

Polarimetry and photometry of the dynamically new comet C/2002 T7 (LINEAR) have given possibility to obtain phase dependence of polarization in WRC filter (λ 7228/1142 angstrem) in the range of negative polarization ($\alpha = 6.4 \div 26.0°$) with the parameters: $P_{min} = -1.63\%$, $\alpha_{inv} = 22.7°$, $h = 0.24$. From the photometry the following characteristics have been obtained: the column density of molecules C_2 in the line of sight $\log N(C_2) = -9.15$ mol/cm^2 and their production rate $\log Q(C_2) = 27.11$ mol/s. The physical parameters of comet C/2002 T7 (LINEAR) are close to the average characteristics of typical dusty comets (Velichko F., Kiselev N., Velichko S.).

Another important aspect of asteroid studies that is developed in our Institute is the electronic Database of Comet Polarimetry that contains more than 2600 measurements of linear and circular polarization for 64 comets starting since 1940. It is a component of the

international Database PLANETARY DATA SYSTEM (NASA) and can be accessible via http://www.psi.edu/pds/archive/comets.html (Kiselev N., Velichko S.).

Physical properties of Transneptunian objects

The recent discovery of Trans-Neptunian objects, called also Kuiper belt objects (KBOs), has opened new horizons in the Solar system study. An entirely new population of planetary bodies has been found, which should contain the most primordial material from the formation of the Solar system. The Kuiper belt objects may be observed only at a very limited phase angle range (usually less than 2°) where the opposition effect plays a dominant role. We made first estimations of the opposition effect amplitude and width based on observations of two KBOs (15789 1993 SC, 20000 Varuna) and one Centaur (10370 Hylonome). They gave first evidence on the existence of a very narrow opposition surge starting at phase angles below 0.1° – 0.2°. Further observations of Varuna confirmed the pronounced opposition surge at phase angles less than 0.1° with amplitude of 0.2 mag relatively to the extrapolation of the linear part of magnitude phase dependence to zero phase angle. The obtained data give a first look into the microscopic properties of the surface layers of TNOs and suggest different surface properties as compared to less distant small Solar system objects (Belskaya I. N.).

4.3. Martian UV Clouds Observed by Hubble Space Telescope in Polarized Light in 2003

Yu. Shkuratov and V. Kaydash

The Hubble Space Telescope (HST) carried out extensive observations of Mars that, for the first time, included polarimetric observations during the close approach to the Earth in August and September 2003. Our Institute was responsible for data processing and analyzing of polarimetric images.

The observations took advantage of the closest Earth-Mars encounter in nearly 60,000 years as Mars passed within 0.372 AU of Earth. The angular diameter of the apparent Martian disk was 25.1 arc seconds. Five series of images of Mars at phase angles about 6, 8, 10, 13, and 16° were taken with polarization filters. Each series consisting of 4 sets of images taken with different wide spectral bands centered at 250, 330, 435, and 814 nm. Each set contains 3 images taken with 3 linear polarization filters, each offset by 60°, allowing complete information of the linear polarization. The

observation moments were chosen so that the same hemisphere of Mars, containing Valles Marineris and contrasting albedo details of Terra Meridiani and surroundings, faced Earth (the disk center is approximately 19°S, 30°E). The High-Resolution Channel of the Advanced Camera for Surveys took the images, having a resolution of 7 km/pixel near the sub-Earth point. This is the highest spatial resolution observations of Mars ever made from the Earth. The Martian atmosphere was relatively free of both dust and water ice clouds during this perihelion observation period. Southern Mars summer occurred at this time.

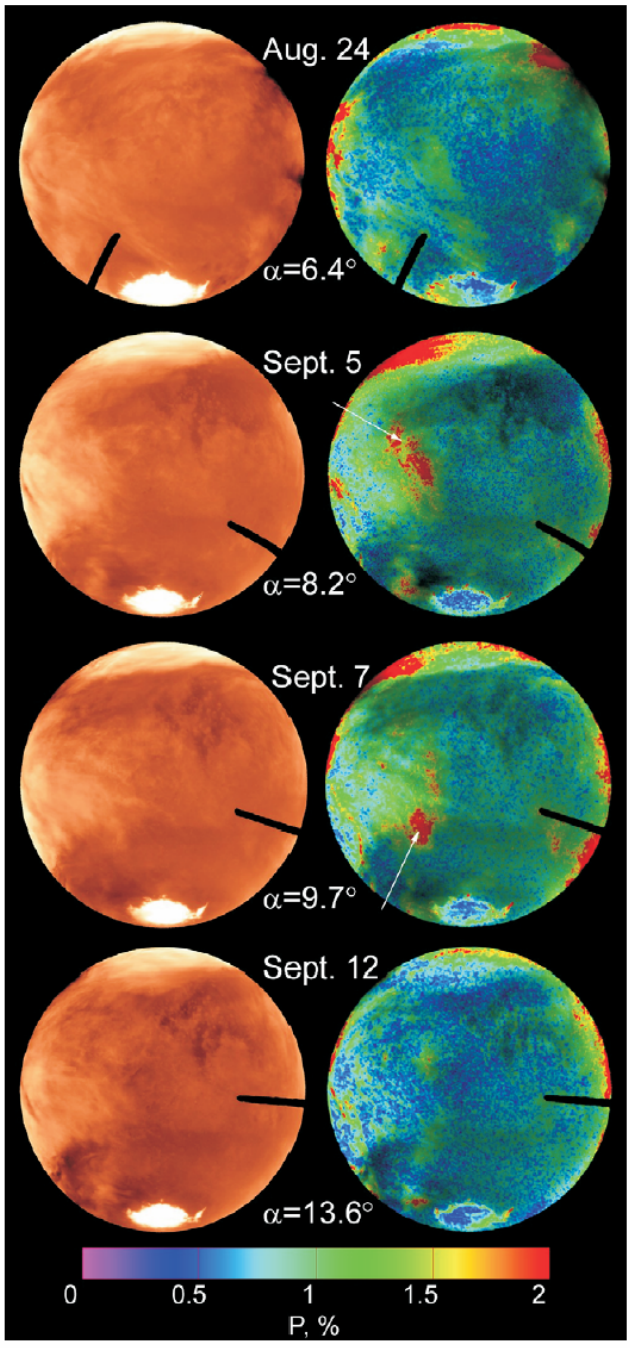

Figure 20. Intensity (left) and polarization degree (right) for Mars on four observation dates of HST (filter F330W). The black coronographic finger and spot are shadowed areas of the detector. The arrows show the polarimetric transient effect.

Linear polarization of scattered light can be described by two parameters, for example, the polarization degree P and the polarization plane position angle ϕ, or normalized Stokes parameters $Q/I = P\cos2\phi$ and $U/I = P\sin2\phi$. Figure 20 presents initial images (left side) and corresponding distributions of polarization degree P (right side) acquired at wavelength 330 nm and the phase angles near 6, 8, 10, and 13°. Coronographic (dark) spots in the field of view obscured a small portion of the disk. All brightness images reveal small surface contrasts and the high-contrast polar areas.

The Martian surface and atmosphere both contribute to the polarization of scattered solar radiation. The surface scatterers are soil particles of different sizes and shapes. The atmospheric scatterers include molecules and sub-micron dust haze particles of the clean atmosphere, faint high altitude mists made of very small aerosols, clouds consisting of dry-ice crystals, and clouds composed of comparatively large dust particles associated with local dust storms.

The South-polar region (bottom) is clearly visible showing gradual decreasing in size with the phase-angle increase during almost a month. The North-polar region is hidden with clouds. Globally, polarization degree of Mars in our observations is ~1% (on average the polarization is negative). Minimal values of P are observed for the south-polar cap and some clouds (< 0.1%). In particularly, the clouds over the North-polar regions have relatively low polarization. The dust storm feature that is observed in the left portion of the disk has polarization lower than that of the surface. This is seen especially at phase angles 13°.

We revealed a new phenomenon, clouds that are only visible in the UV with polarized light. This new type of clouds with P as high as 2% are located in the left part of the disk in the images acquired at 8 and 10° (see arrows). The clouds are located at the edge of a dust storm. They also are seen in other UV filters, but the contrast of the clouds is highest at λ = 330 nm. We suggest that this could be a zone of ice condensation on small dust grains. Being almost invisible at the moment corresponding to α = 6°, the cloud appeared in a few days and shifted to the south limb during a week and then disappeared. The most interesting feature of such clouds is that they are almost transparent. The surface albedo pattern remains visible through them with almost no attenuation even in the UV spectral band. Thus, they are recorded by their polarization only.

Thus, the HST observations that were designed to obtain maps of surface scattering properties have led to the discovery of a new type of clouds, the UV polarimetric clouds that are transparent and can be revealed only with polarimetric measurements.

Further analyses of these results promise a new insight into microphysics of aerosols with possible wide implications to global climate models of Mars.

4.4. Jupiter's Atmosphere

O. S. Shalygina, V. V. Korokhin, E. V. Shalygin, G. P. Marchenko, Yu. I. Velikodsky, L. V. Starukhina, O. M. Starodubtseva, and L. A. Akimov

As is known, ground-based and cosmic polarimetric observations of Jupiter in the visual spectrum range show increasing of linear polarization with latitude (even at zero orbital phase angle). Polarization degree increases from zero (equatorial regions) up to 7-8% (polar regions). Also it is known, that there is a north-south asymmetry of linear polarization at Jupiter [e.g. Gehrels et al., Astron. J. 1969. 74, 190].

To explain these observational facts, we started regular polarimetric observations of Jupiter with the 0.7 m telescope AZT-8 of our observatory. Figure 21 shows an image of Jupiter acquired in blue filter; Figures 22 and 23 present polarization degree and angle of polarization plane distributions, respectively. One can clearly see the polar effect.

On the basis of our earlier observations near oppositions during 1981-1999, seasonal variations of north-south asymmetry (P_N-P_S) of linear polarization *P* in polar regions and some relation between P_N-P_S and insolation have been found. The parameter of asymmetry P_N-P_S is defined as a difference between values of linear polarization degree on north and south at the latitudes ±60° at the central meridian. Addition of new observational data (2000-2004) and joint analysis with previous data allowed us to find anticorrelation between asymmetry of Jupiter's polarization and insolation (see Fig. 24). Correlation coefficient between P_N-P_S and I_N/I_S is -0.7, i.e. there is significant anticorrelation. Thus, we can speak about seasonal variations of polarization.

We assume that variations of insolation (through temperature changing) are the principal cause of the seasonal variations of polarization. Jupiter has a small axial tilt (about 3 degrees). However, the orbital eccentricity about 0.05 results in 20% variations of Jupiter surface illumination due to the change of the distance *r* from the Sun. Besides, the perihelion and maximum of Jovian latitude of the Sun are almost coinciding in time. These factors produce seasonal fluctuations of the incident solar radiation and result in north-south asymmetry in insolation and temperature. Seasonal variations of stratospheric temperature at the polar regions in Jupiter's atmosphere are ±25°K.

Observational data and theoretical modeling indicate the presence of thin aerosol layer in stratosphere on p ~ 20 mbar pressure level with greatest abundance at the polar regions; this haze conceivably consists of benzene and polycyclic aromatic hydrocarbons (PAH) like naphthalene, phenanthrene, pyrene [Friedson et al. Icarus 2002. 158, 389]. Most likely, aerosols of this haze are in unstable state and temperature changing may influence on generation/dissociation of particles.

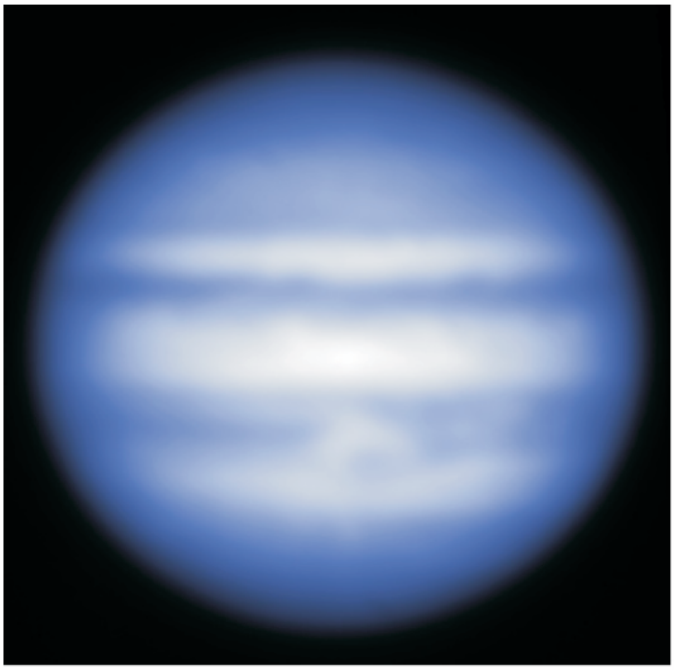

Figure 21. Image of Jupiter at λ = 456 nm obtained 1998.09.10 in opposition with telescope AZT-8 of Chuguev observational station of Institute of Astronomy, Kharkiv National University.

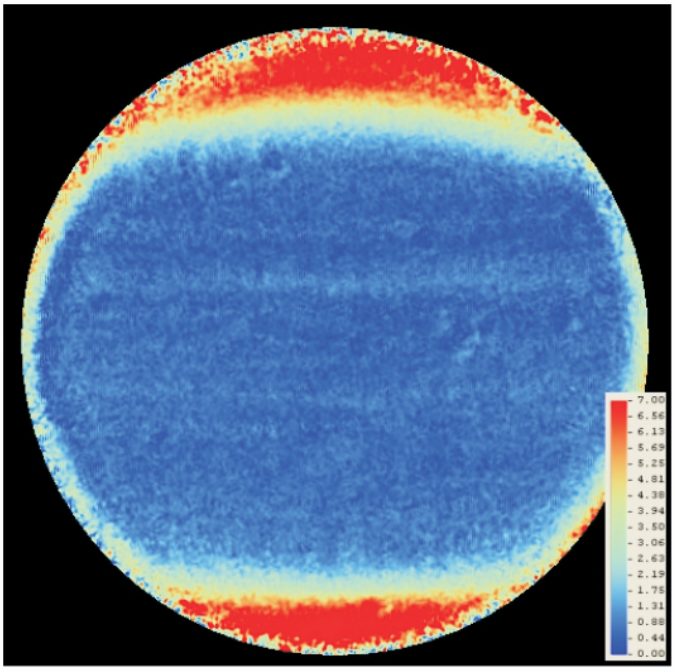

Figure 22. Distribution over Jupiter's disk of linear polarization degree in opposition at λ = 456 nm

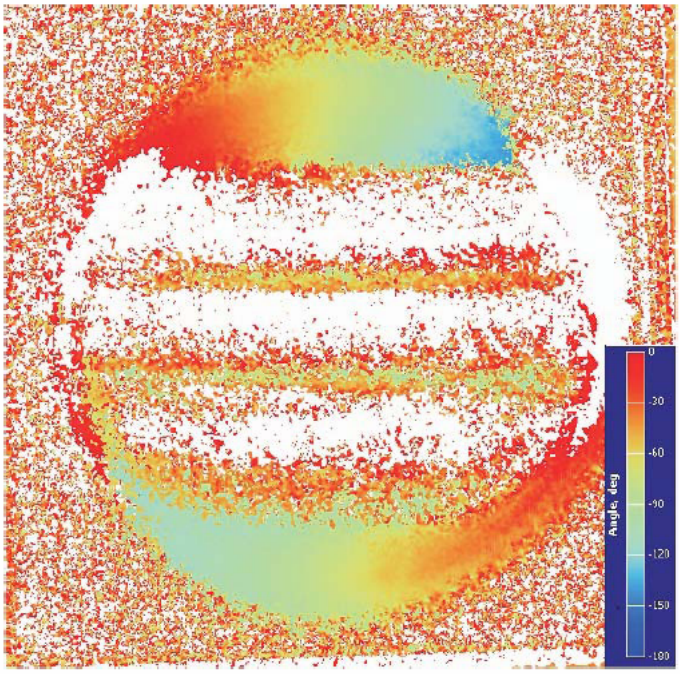

Figure 23. Distribution over Jupiter's disk of angle of polarization plane in opposition at λ = 456 nm

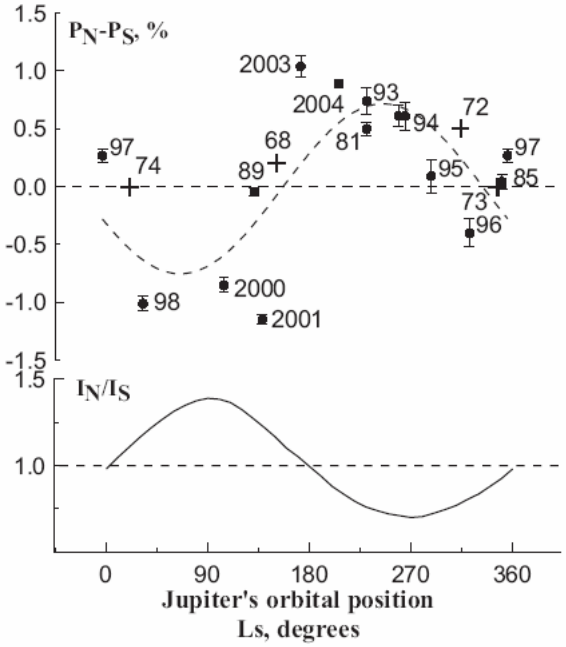

Figure 24. Dependence of North-South asymmetry of P_N-P_S on planetocentric orbital longitude of the Sun Ls (upper plot). Dashed line is approximating curve: P_N-P_S= -0.67sin(L_S+0.32)+0.05. Solid line is theoretically calculated asymmetry of insolation of polar regions (intensity ratio I_N/I_S at latitudes 60°)

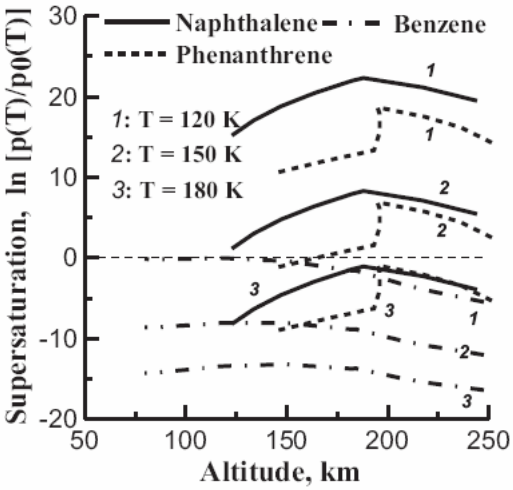

Figure 25. Altitude distributions of PAH supersaturation for different Jovian temperatures

The P_N-P_S values and its anticorrelation with insolation may be caused by seasonal variations of insolation and temperature. Our estimates show (Fig. 25) that temperature changes have strong effect on processes of homogeneous nucleation in Jupiter's stratosphere: benzene does not condensate at T>120°K (negative supersaturation means

vapor undersaturation), whereas probability of naphthalene and phenanthrene nucleation at T=120°K and T=150°K is considerable. Average temperature in polar regions of Jovian stratosphere is about 150°K. This temperature is lower than triple points of naphthalene and benzene (359°K and 278°K, respectively), so they may produce crystal nucleus from gaseous phase. Particles of the evaporating naphthalene and phenanthrene substances may be formed by homogeneous nucleation and are the centers of condensation of different evaporating substances.

Also we note probable influence of solar cosmic rays (protons, E>10 Mev) flux on concentration of aerosol haze particles through series of chemical reactions that produce source material for aerosol formation.

4.5. Light Scattering by Particles and Particulate Surfaces

Yu. G. Shkuratov, E. S. Zubko, V. A. Psarev, A. A. Ovcharenko

We present here results from photometric and polarimetric measurements of laboratory samples (that simulate the structure of planetary regoliths) to DDA and T-matrix simulations of light scattering by small particles with various shapes.

1. Various models have been used to simulate non-spherical dust particles occuring in nature. We use the Discrete Dipole Approximation (DDA) technique exploiting our well-tested DDA code. According to the DDA approach a particle is represented by an array of dipoles densely filling the particle volume. Then the integral equation rigorously describing light scattering by such an array is converted into a system of linear algebraic equations. We solve this system by the method of conjugate gradient using the fast Fourier transformation. Figure 26 shows examples of light scattering agglomerated particles. Actually only the DDA technique allows one to compute scattering properties of such debris particles. Intensity and linear polarization degree are given in Fig. 27 as functions of the phase angle and size parameter $x = 2\pi r/\lambda$ (r and λ are the radius of the circumscribed sphere and wavelength, respectively) for agglomerated debris particles. Panels (a)–(c) correspond to the following refractive indecies: $m = 1.5 + 0.1i$, (organic), $m = 1.6 + 0.0005i$, (silicate), $m = 1.31 + 0i$ (icy materials). Calculations made for different refractive index, clearly manifes the evolution of the negative and positive polarization branches with change of the size parameter.

Figure 26. Example of irregular agglomerated debris particle

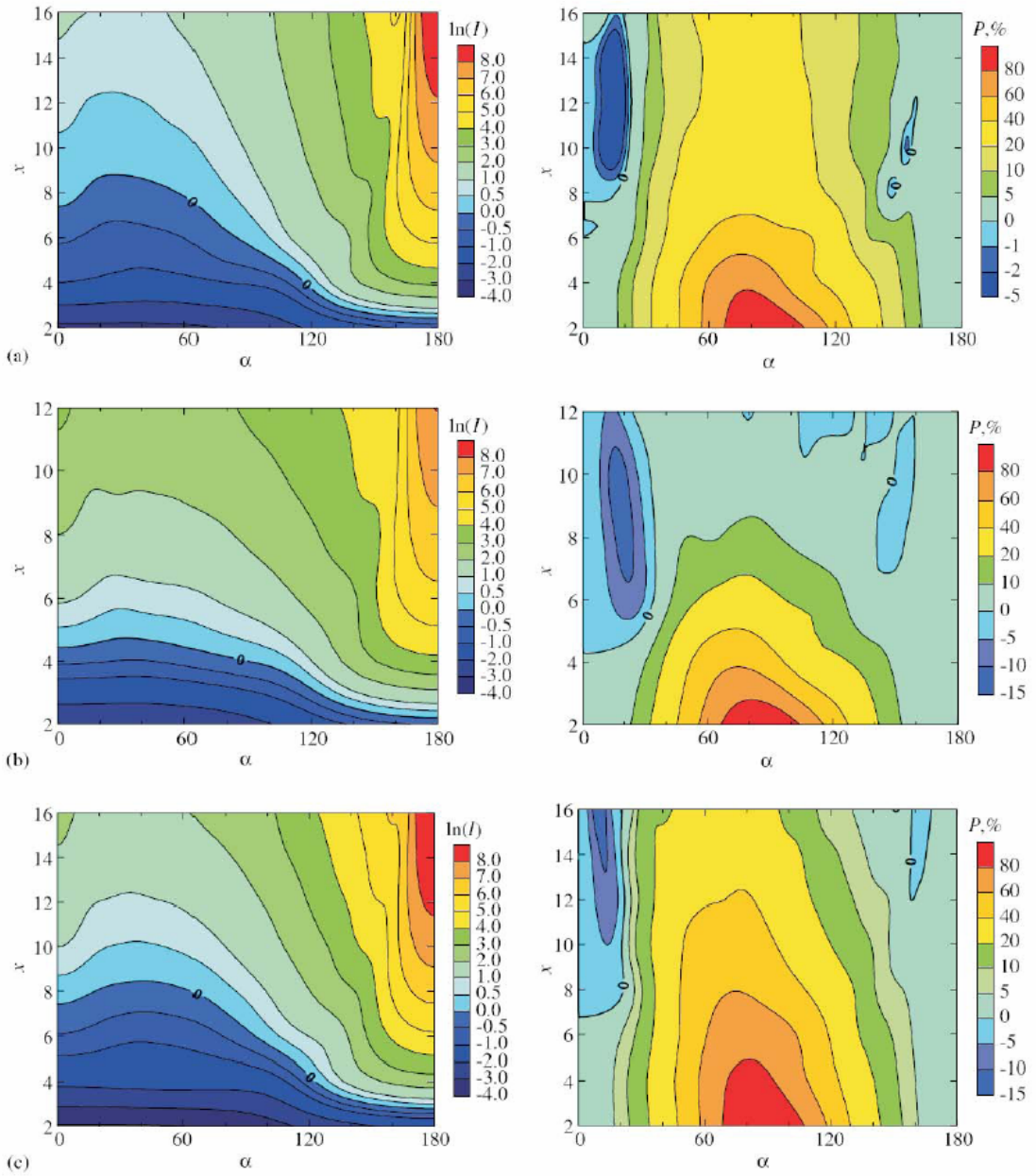

Figure 27. The maps of intensity and degree of linear polarization as a function of the phase angle and size parameter for agglomerated debris particles. Panels (a)–(c) correspond to organic, silicate, icy materials

2. The laboratory studies of structure simulants of planetary regolith are carried out with three instruments operating at small phase angle ranges covering 0.008 – 1.5° (laser photometer) and 0.2 – 17° (lamp photometer/polarimeter) and wide phase angle range 2 –

150° (lamp photometer/polarimeter). The last two instruments allow measurements at wavelengths of 0.63 and 0.45 μm with unpolarized incident light. Note that the phase angle range < 2° is very poorly studied. One of the purposes of our laboratory studies is brightness and polarimetric opposition effects ubiquitously observed in nature for particulate (regolith-like) surfaces. We studied a range of samples that are characterized with a variety of mechanical structures and albedo. A strong particle-size dependence of the negative branch of polarization for powdered dielectric surfaces was found: the larger the particle size, the narrower the opposition spike and the negative polarization branch. In Fig. 28 we show an example of measurements of a sample of red clay carried out with the instrument that covers the angle range 2 – 150°. The plot allows one to compare photometric and polarimetric phase dependencies for particles in air (single scattering) [Volten et al. JGR 2001. 106. 17,375] and when particles form a particulate surface (multiple scattering) at the two wavelengths. Figure 28 prsents data for compressed and uncompressed particulate surfaces. Analysing of these data clearly show that the main cause of the negative polarization of particulate surfaces is single particle scattering.

Figure 29 illustrates results of our measurements obtained with the laser photometer covering the angle range 0.008 – 1.5°. One can see 3 normalized photometric phase curves measured at λ = 0.63 μm: fine powders of MgO (very bright surface), carbon soot (very dark surface), and glass spherical beads with the diameter of particles near 50 μm (bright surface). Bright samples demonstrate narrow spikes of backscattering related to the coherent backscatter enhancement effect. The spherical beads also show several resonances. The measurements are used for interpretation of photometric properties of Kuiper Belt objects.

4.6. Implanted Gases on Atmosphereless Celestial Bodies

L. V. Starukhina

The interest for solar wind implanted gases is due to the prospect of extraction of potential thermonuclear fuel ^{3}He, as well as to the fact that implanted hydrogen can be ascribed to water in different types of remote sensing experiments.

Implanted hydrogen in lunar regolith

The surfaces of airless celestial bodies are exposed to energetic protons – mainly to solar wind protons of keV range. They provide severe radiation damage in the rims of

regolith particles creating trapping sites for the implanted solar wind ions. In silicates, important case of trapping sites are broken chemical bonds of oxygen atoms; they tend to be saturated by the implanted H-atoms so that OH-bonds are formed [e.g., Zeller et al. JGR. 1966. 71. 4855]. Irradiation-induced OH-groups were found by optical absorption near 3 μm, which is due to O-H stretch of hydroxyl groups. Thus, the implanted protons can be detected by optical spectroscopy near 3 μm and be mistaken for OH groups in water molecules.

Our estimates of the upper limit of concentration of solar wind hydrogen trapped per unit area of rims of lunar regolith particles, in particular, in OH groups, yield $n_s \approx (1 \div 5) \times 10^{17}$ cm^{-2}. This is in agreement with laboratory experiments. Mass fraction of the implanted hydrogen [H] = $Sm_p n_s$ for typical specific surface area of regolith S = 800 - 5000 cm^2/g (m_p is proton mass) is at least 130 ppm, but even the maximum [H] = 1700 ppm found in neutron spectrometry experiment on Lunar Prospector [Feldman et al. JGR. 2001. 106. 23,231] can be achieved at moderate values of $n_s = 2 \times 10^{17}$ cm^{-2}. If this hydrogen is interpreted as a constituent of water ice, its weight fraction can be up to a few wt.%. Thus, the excess hydrogen found on the Moon can be of solar wind origin and not belong to water molecules.

Optical effects of solar-wind-induced OH

A 3-μm absorption band was observed in reflectance spectra of asteroids of different taxonomic classes, including E and M types supposed to be differentiated and hence dehydrated. This unexpected absorption can be due to OH-groups of solar wind origin. We simulated this effect on the base of our model of spectral albedo of multicomponent regolith-like surface. The model enabled us to calculate the change in reflectance of featureless continuum when rims of regolith particles contains OH-groups. Simulated 3-μm bands are presented in Fig. 30. It shows that, if the variance of spectral positions of OH absorption maxima near different cations is taken into account, neither depth nor width, shape and position of 3-μm band can be used to distinguish between H_2O molecules or true hydrosilicates and OH-groups of radiation origin, at least at low band depths (which is the case for most observations). In Fig. 31 calculated 3-μm depths of irradiation origin are compared with those observed for asteroids, OH-concentration taken about the upper limit. Fig. 31 shows that only 3-μm bands of Pallas, Ceres, and Virginia are deeper than it could be due to solar wind OH, and thus can be interpreted as due to hydrosilicates. Calculations of band depths due to 1wt.% water ice (Fig. 31) show

that fine ice particles can contribute to 3-μm absorption much stronger than solar wind OH, and the contribution of coarse ice particles would be negligible.

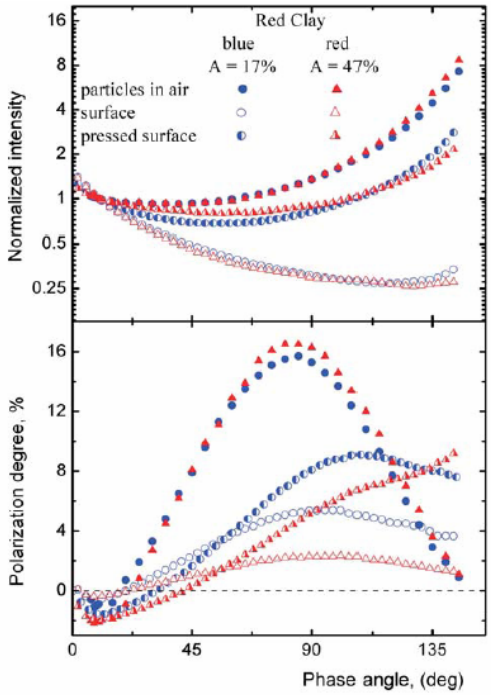

Figure 28. Photometric and polarimetric phase curves for particulate surfaces (compressed and uncompressed) and aerosol particles measured at λ=0.44 and 0.63 μm for the red clay powder. The intensity is normalized to unity at the phase angle 10°

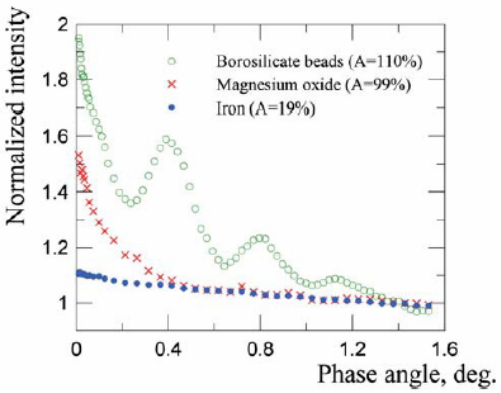

Figure 29. Normalized photometric phase curves of 3 samples measured at λ= 0.63 μm. The normalizing angle is 1.5°

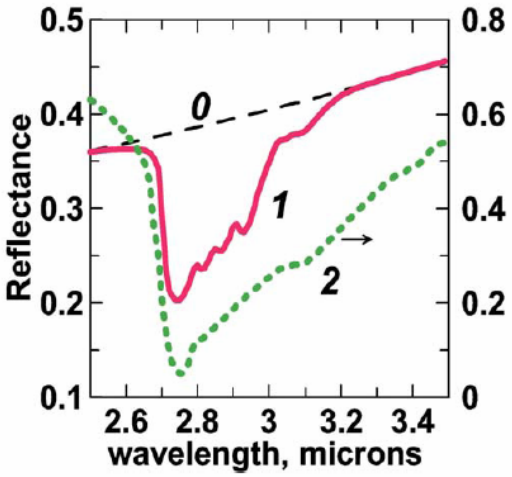

Figure 30. Simulation of effects of hydroxyl of solar wind origin (*1*) on a featureless spectrum (*0*). For comparison, 3-m band of montmorillonite (*2*) is shown (its scale is on the right)

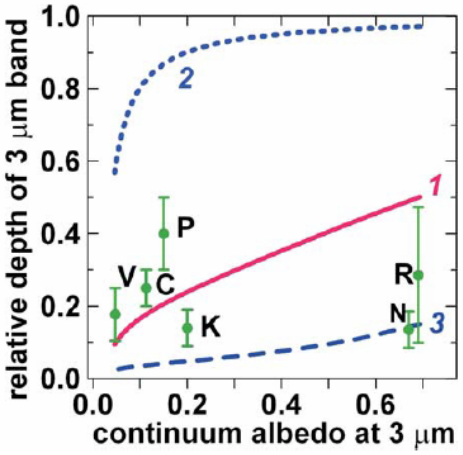

Figure 31. Calculated normalized depths for the solar-wind-induced 3 μm bands of complicated shapes (*1*) and for 1 wt.% of fine (*2*) and coarse (*3*) ice particles vs. surface albedo. Points present the deepest 3 μm band depths for asteroids: Virginia (V), Ceres (C), Pallas (P), Roxane (R), Kalliope (K), and Nysa (N)

Distribution of solar wind implanted gases: the effect of temperature and material

The implantation origin of the hydrogen detected on the Moon by Lunar Prospector is supported by the observed regional variations of the excess hydrogen. They are of two

types: (1) global, temperature-correlated, excess H being concentrated in the polar regions; (2) local spots of excess H in equatorial regions and lack of H in some permanently shaded areas. The local variations cannot be explained by ice hypothesis; both types of variations are consistent with the implantation hypothesis.

Saturation of a particle on the lunar surface with H-atoms takes ~10^2–10^3 years, which is much shorter than solar wind exposure of the particles, so even polar regions are saturated with the implanted hydrogen, the Earth magnetosphere being the source of protons for permanently shaded areas. Therefore, H-abundance is controlled by degassing processes. Their rate is extremely sensitive to temperature: ~exp(–*U*/*kT*). At low temperature, the implanted atoms become “frozen” into the regolith particles, which provides global [H] trend. Variations of trapping energies *U* with mineral type as well as thermal and irradiation history can provide selective gas accumulation or degassing and irregular local features: high U are responsible for excess H in “hot” regions and low U can account for lack of H in cold areas.

A similar global and local distribution can be expected for the other solar-wind-implanted elements, e.g., for ^{3}He. Thus, polar regions of the Moon are the most promising place to extract this potential thermonuclear fuel.

4.7. Solar Studies

L. A. Akimov, I. L. Belkina, V. V. Korokhin, G. P. Marchenko

Our Institute is the International Solar Station № 34501 carrying out monitoring of solar activity in the chromospheric line H_α. Data on solar flares, active prominences and eruptive events are obtained, processed, and sent to World Data Center WDC Boulder Co, USA. From 01.01.2001 to 12.31.2007 data about 395 solar flares and 356 eruptive events have been obtained.

Kharkiv spectroheliograph has been equipped with a CCD-camera. This provides for higher angular resolution, especially in IR. After the modernization, the spectroheliograph allows us to record the images of the Sun in any spectral line of the 350 – 1100 nm range in 2 minutes. Figure 32 shows an image of the Sun in He I line (10830 angstrem) obtained with the spectroheliograph, 2007.08.25. Figure 33 shows comparison of images of the Sun in He I line acquired in our Institute (2007.08.17, UT 11^h09^m) and National Astronomical Observatory (Kitt Peak) (2007.08.17, UT 18^h07^m).

We support several web-sites presenting regularly updated solar activity data. One of them (http://www.astron.kharkov.ua/khassm/) presents solar images at different wavelengths, which have been obtained at our observational station. Web-site “Space Weather” (http://sw.astron.kharkov.ua/) uses space data and after our processing represents in real time information about Earth space environment (X-flares, proton events, and Kp that is the geomagnetic index) in friendly graphic form.

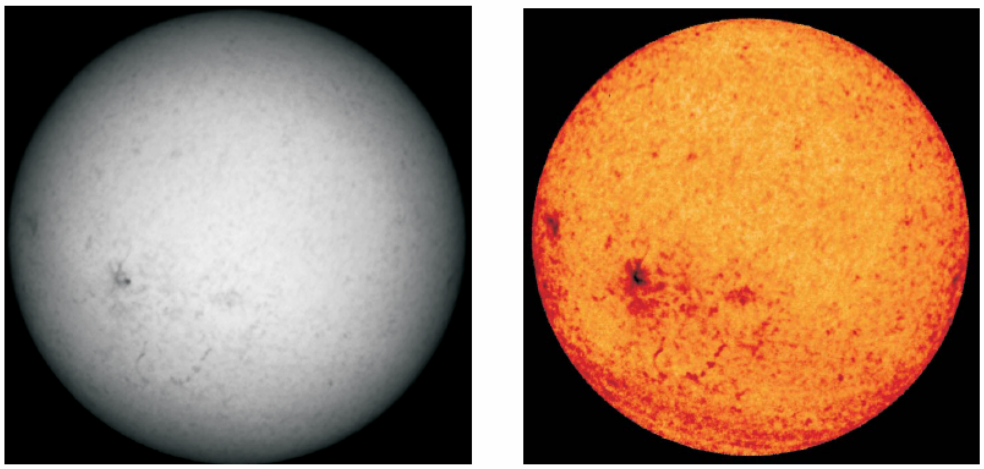

Figure 32. Image of the Sun in He I (10830 angstrem) line, 2007.08.25. Left: before darkening compensation, right: after darkening compensation

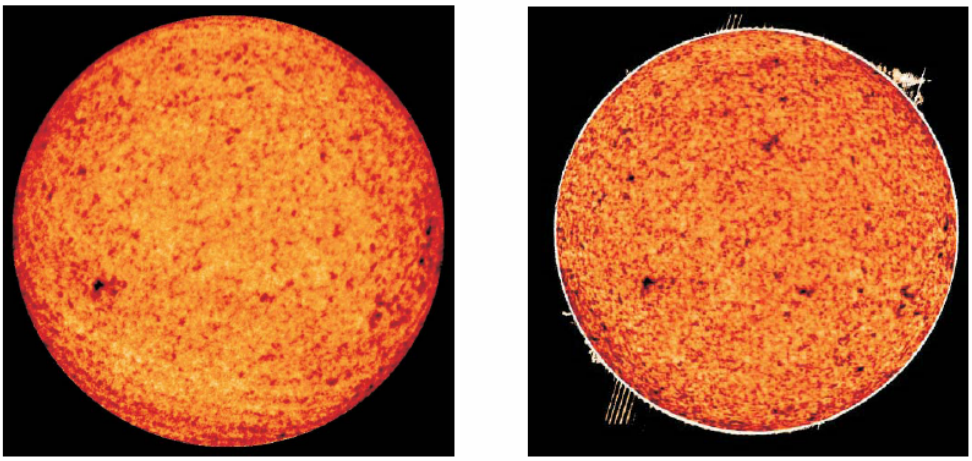

Figure 33. Image of the Sun in He I (10830 angstrem) line, 2007.08.17. Left: Institute of Astronomy, Kharkiv National University, UT 11h09m; Right: NAO (Kitt Peak) UT 18h07m

We carry out solar cyclic researching using data on X-ray flares. Daily flare indexes *XFI* have been calculated for time period from 01.01.1975 to 31.12.2007. Using the *XFI* index, it has been demonstrated that the maximum of the current 23-rd solar cycle was smoother than for the previous cycle. It has been found that full energy of all solar flares in

the 22-nd cycle was in 2.5 times greater than energy of the 23-rd cycle. We have found difference between the 22 and 23 solar cycles in power spectrum of these periods.

Maps of distribution of surface brightness of the chromosphere in D_3 line of helium along latitude as a function of altitude have been studied for three solar eclipses. It has been found that heterogeneity of distributions of the lines intensity has the typical size of about the supergranulation size. It has been shown that height distribution of the surface brightness of chromosphere in the D_3 HeI line has one or two maxima at the altitude ~200 km (lower) and 1500 – 2000 km (basic). The lower maximum is explained by coronal X-ray radiation with wavelengths less than 6 nm that causes helium ionization. It has been shown that such a coronal emission may reach of photospheric altitude. The results found from eclipse of March 29, 2006 data confirms our assumption that lower maximum of the altitude distribution of helium is absent during solar activity minimum.

Quasi-synchronism of X-ray bursts in the structures of solar corona in the Mg XII 0.84 nm line from the SPIRIT/CORONAS-F data was studied. It has been revealed that the sympathetic bursts are observed in some pairs of AR fragments. The probable values of magnetic field strength are 65 – 410 Gs if the related sympathetic bursts are caused by propagation of MHD waves in the coronal loops.

During 3 years in different seasons, studies of atmospheric vibrations of the solar limb at the Chuguev Observational Station were carried out using a specially developed device. It has been shown that mean-square amplitude of image tremble is within 1″ for 70% cases of the researching period. In summer, during stable anticyclone, the amplitude is within 0.9″, and in the morning and evening times is about 0.5″ - 0.6″. It allows us to carry out high-quality observations of the Sun at the observational station using new spectrogeliograph which is constructed at Institute for Radiophysics and electronics of National Academy of Sciences for our Institute.

4.8. Gravitational lenses

V. Dudinov, V. Vakulik, V. Tsetkova, V. Konichek, A. Zheleznyak

If the light rays from a distant source (e.g., a quasar) pass close to a massive body (e.g., a galaxy) in their propagation to the observer, a gravitational mirage arises: the observer may see either a ring, or an arc, or two or four images of the same source. This is a phenomenon of gravitational lensing, which is one of the predictions of the general relativity theory. It can arise at different spatial scales, from microlensing of stars by

compact bodies populating our Galaxy (galactic microlensing) to gravitational lensing of quasars by foreground galaxies (strong lensing) or by remote galaxy clusters (weak lensing). The gravitational lensing phenomenon is presently believed to be a powerful tool to solving a number of fundamental problems of the contemporary astrophysics and cosmology, with the problem of dark matter being the most important one. According to the current conception, a contribution of the dark matter into the cosmological density is large enough, but its composition, properties, and distribution in the Universe remains to be unknown.

Because of gravitational focusing, distant quasars are observed split into two or more images. If some of the lensed images are observed through the densely populated regions of lensing galaxies, microlensing events can be observed, which occur in passing microlenses (planets, stars and stellar-like bodies) near the line of sight. Microlensing light curves contain extremely valuable information about masses and velocities of microlenses which cause these events, as well as about spatial structure of quasars' emitting regions with a resolution unachievable to other methods.

One more important astrophysical application of investigation of gravitationally lensed quasars (GLQ) should be noted. While propagating through the lensing galaxy along different paths corresponding to different lensed images, the light rays from the source quasar come to the observer with different time delays. Knowing of the time delays between the quasar intrinsic brightness variations provides an independent way to estimate the most important cosmological parameters of the Universe, such as the Hubble constant and deceleration parameter.

As a rule, GLQs are faint and extremely compact objects with a rather complicated spatial structure: for the majority of GLQs, two or four lensed quasar images and an image of a lensing galaxy are situated within a very small sky area, up to 2″ or even less. This makes high demands on the initial image quality and needs complicated algorithms of photometric image processing. Thus, such objects could attract a keen interest of researchers who have accumulated a great experience in developing methods of high resolution imaging for astronomy, namely speckle interferometry of red giants, binary and multiple stars, speckle imaging, and applications of the developed methods to processing images of asteroids and major planets (Dudinov V., Kuzmenkov S., Tsvetkova V., Konichek V., Pluzhnik Ye., Vakulik V., Zheleznyak A.).

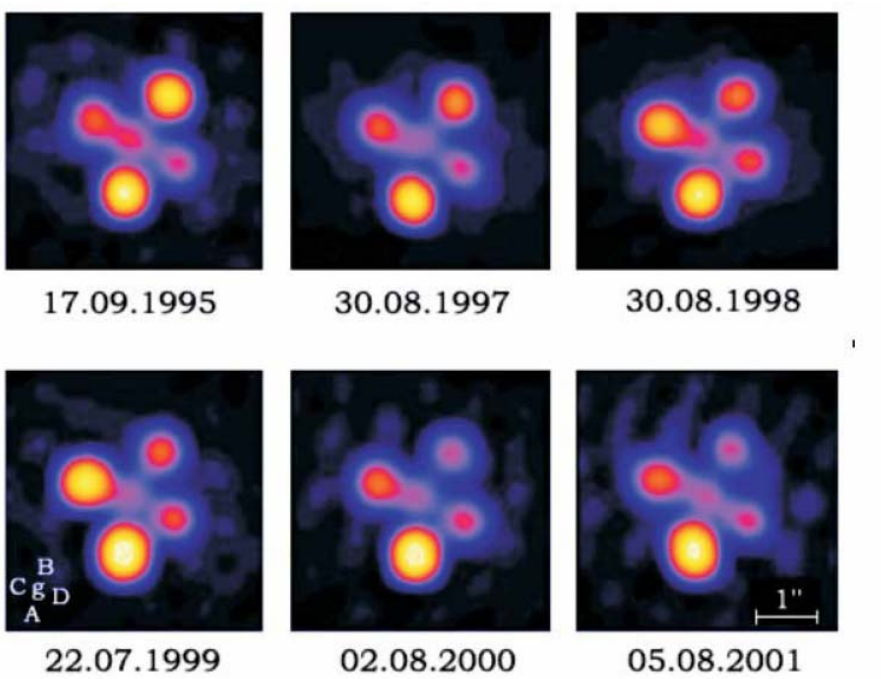

Figure 34. Images of gravitationally lensed quasar Q2237+0305 (Einstein Cross), obtained in VRI filters July 22, 1999 with the 1.5 m telescope at Maidanak observatory

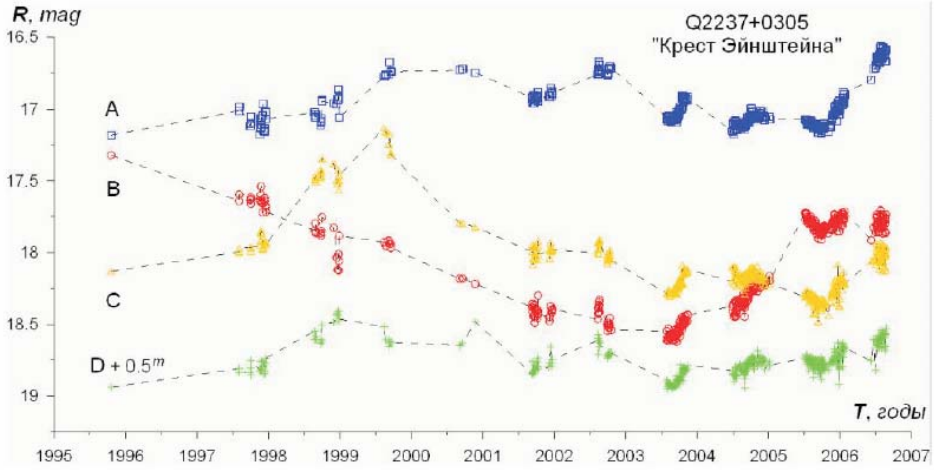

Figure 35. Results of photometry of the quasar Q2237+0305 (Einstein Cross), obtained in 1995-2006 years in filter R with the 1.5 m telescope at Maidanak Observatory (see Fig. 34)

Regular observations of GLQs with the 1.5-m telescope of the Maidanak Observatory (Central Asia) were started by workers of our Institute in 1997. The telescope with the diffraction quality optics, a modern CCD light detector, extremely good seeing conditions, and a large number of cloudless nights have made it possible to obtain a huge amount of superb observational data on a number of GLQs, with an emphasis on the Q2237+0305, Q0957+561, SDSS0909+532 and SBS 1520+530 systems.

During 2003-2007, the results of the long-term observations of these systems with the Maidanak telescope were being summarized. In particular:

1. For Q2237+0305, the Einstein Cross (see Fig. 34), a significant positive correlation between the variations of color indices and magnitudes of the lensed quasar images has been discovered, in the sense that the images tend to become bluer as their brightness increases. This microlensing-induced phenomenon, which has never been investigated earlier, is of a great diagnostic importance both for study of quasar spatial structure and for examining the physical state of the matter emitting by various quasar regions. The results allowed us to propose a new two-component model of the quasar Q2237 spatial structure consisting of a compact central source surrounded by an outer extended feature, with the central source contributing from 20% to 10% in the spectral bands from V to R, respectively. The quasar central source dimensions were estimated to be about $2 \cdot 10^{15}$ cm, provided that the transverse velocity is 5000 km/s, (V. Vakulik, V. Dudinov, V. Konichek, A. Zheleznyak, I. Sinelnikov).

The time delays between the quasar brightness variations seen in the lensed images of Q2237+0305 were estimated for the first time for this system in the optical wavelengths. The upper limits for time delays of B, C and D components with respect to A of order of three days were obtained. This has become possible thanks to observations of June-October, 2003, when the quasar intrinsic brightness variations revealed themselves in fact for the first time since the system discovery in 1985. Figure 35 presents results of photometry of the quasar Q2237+0305 (Einstein Cross) carried out in 1995-2006 years in filter R with the 1.5 m telescope at Maidanak Observatory (the component A – D are shown in Fig. 34). Figure 36 shows comparison of our photometric data for the quasar Q2237+0305 and data obtained in the frame of the programe OGLE III, revealing good resemblance.

2. For SDSS 0909+532, the first successful time delay measurement has been made for this system with the use of the joint observations at the 1.5-m telescopes in Maidanak and Calar Alto observatories (A. Zheleznyak, in collaboration with Ullán A. Goicoechea L. from the Calar Alto Observatory).

3. For Q0957+561, interpretation of the data obtained together with the Harvard-Smithsonian Center for Astrophysics (USA) in the framework of the international Quasar Observing Consortium (QuOC) program was fulfilled (W. Colley, R. Schild, V. Dudinov, A. Zheleznyak). The program permitted us to obtain a new more exact estimate of the time delay between the quasar brightness fluctuations seen in the two lensed images (417.09±0.07 days). Also, extremely short-time microlensing brightness variations (several days) of very small amplitudes, 0.04^m-0.05^m, caused seemingly by planetary

mass objects have been revealed and successfully interpreted by a new physical model of the quasar (V. Vakulik, in collaboration with R. Schild from the Harvard-Smithsonian Center for Astrophysics).

4. For SBS 1520+530, new accurate estimates of the R and I stellar magnitudes of the lensing galaxy have been obtained, with the R estimate being taken for the first time for this object (A. Zheleznyak, A. Sergeyev). A numerical simulation allowed estimating the mass of the lensing galaxy and a parameter, describing the mass distribution, which are in a good agreement with the system geometry and the observed relative magnification factor. Both the mass obtained and the measured (H-R) color index indicates that the lensing galaxy is a spiral one. The analysis of light curves in the V, R, and I bands covering the time period from 2001 to 2006 allowed us to confirm the time delay value measured previously and to detect microlensing brightness variations, which allowed us to obtain the first estimate of the source size for this system (~10^{15} cm).

4.9. Globular Cluster M15: New Variable Stars

A. P. Zheleznyak

The search for variable stars in crowded stellar fields is important but at the same time difficult problem, especially for extreme dense objects like centers of globular clusters. It will suffice to mention that in the central part of globular cluster M15 up to the middle of nineteen of XX century only one variable star was known. A new approach to the problem of detection of variable objects in dense stellar fields was developed recently by Alard and Lupton in the area of galactic microlensing searches. The proposed method of optimal image subtraction (OIS) is used for processing of temporal sequences of CCD images of the same stellar field. The main problem in implementing of an image subtraction approach – coregistration of the reference and current images – is elegantly solved with OIS algorithm and allows one to obtain a difference close to the optimal, i.e. the method is limited only by photon noise.

The goal of our work was to implement the OIS method for investigation of globular cluster central parts. The globular cluster M15=NGC7078 was chosen as the target; it is known as the most dense and massive Galaxy cluster with the highest central star crowding. According to estimation with HST, the number of stars brighter that 19^m in the central part of M15 is 15-20 per square arcsecond. Totally, around 150 variable stars was

known in the region of M15; overwhelming majority of the new variables in the densest central (r < 20″) region of M15 have been discovered in the last decade with HST [AJ 106, 154] and 4.2 meter William Hershel telescope, equipped with adaptive optic system.

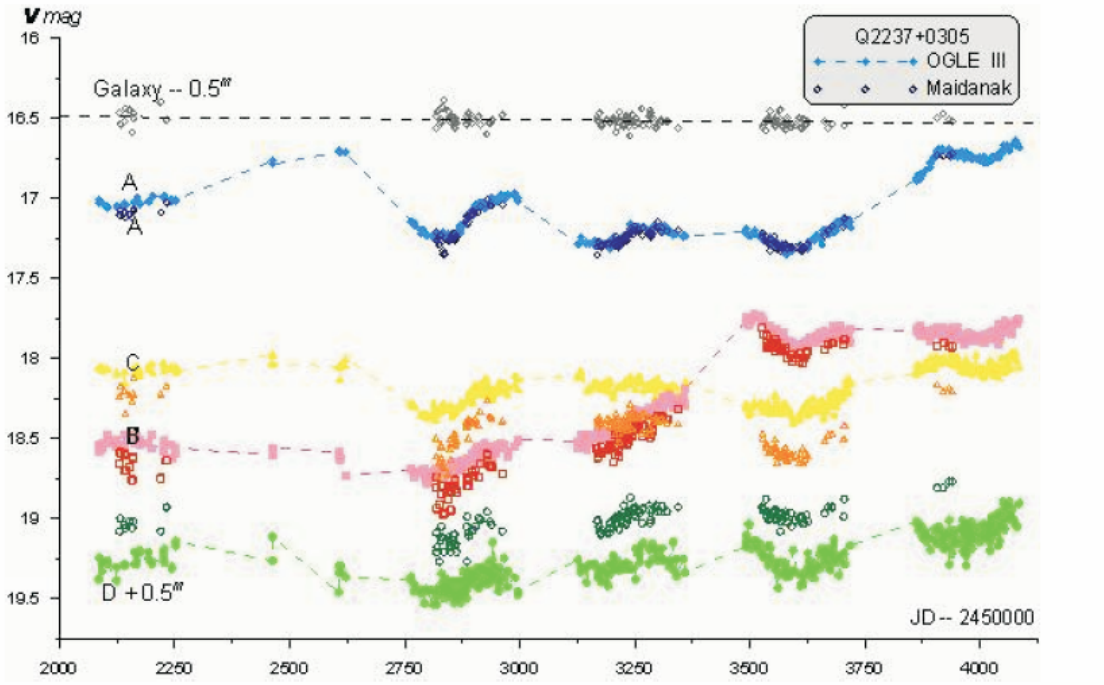

Figure 36. Comparison of our photometric data for the quasar Q2237+0305 (2001-2006, filter V) and data obtained in the frame of the programe OGLE III (see Fig. 34)

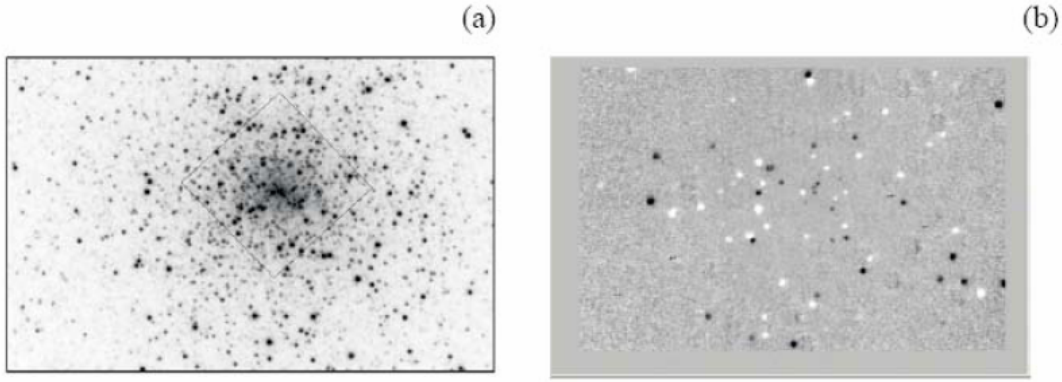

Figure 37. (a) One of CCD images of the globular cluster M15=NGC7078, obtained with 1.5 m telescope at Maidanak observatory on July 31, 2001 in R band. North is on the top; the seeing (FWHM) =0.60″. The intensity was logarithmically scaled to show inner and outer parts of the cluster simultaneously. The square shows the size and orientation of field of view of HST WFPC1 CCD chip. (b) The residual image, in the same scale and orientation as the image (a), obtained after processing of sequence of M15 CCD images with the algorithm of optimal image subtraction. Stars with variable in time intensity are clearly revealed as brighter or darker spots on relatively uniform grey background. Besides variable objects, some CCD defects (of evidently non-pointlike nature) became apparent in the residual image after subtraction

Our observation were carried out with the 1.5 m AZT-22 telescope at Maidanak observatory (Uzbekistan) during two consecutive nights (July 31 and August 1, 2001). The

detector (ST-7 CCD camera) was used in the short–focus mode of AZT- 22, giving the pixel size 0.15″ and field of view 115″×77″. The obtained observational data contain 248 CCD frames of M15 with exposure time 60 sec in R band. The seeing condition (FWHM), estimated from isolated star images in each frame, was practically subarcsecond for the whole volume of data; an appreciable fraction of images has a seeing FWHM < 0.6″. At the first stage all the data passed the standard procedures of astronomical CCD image processing. After implementation of the code, based on the OIS algorithm, 83 variable objects were found in the field of view, 55 of which were identified with the known cluster variables, and 28 are the candidates for the new variable stars. The typical CCD image of M15 from our dataset and the result of processing of the sequence of frames with the OIS method are given, respectively, in Fig. 37 a,b. Most of the newly discovered variables were classified as the RR Lyrae type; two of them most likely are of SX Phe type. Due to relatively high coordinate accuracy of obtained results, during the identification work it was possible to refine the coordinates of already known variables, as well as to correct some errors in the M15 variable stars catalogue. Considerable part of the newly discovered variables (18) are located in the most dense part near the center of M15; here we were able to rediscover all the variable stars, previously found with HST [AJ 106, 154] and almost all of the stars, found with 4.2 m WH telescope. The comparison between HST and our variable coordinates is given in Fig. 38; for convenience, the coordinates of variable stars in ST-7 coordinate system were transformed to the pixel coordinate system of HST WFPC1 chip.

4.10. The Kharkiv's XC1 catalogue of positions and proper motions of faint stars around extragalactic ICRF sources

P. N. Fedorov, A. A. Myznikov

We present a new astrometric catalogue of faint reference stars around ICRF sources of northern hemisphere. The XC1 catalogue was created at our Institute. This catalogue contains the positions and proper motions in ICRS/Tycho2 system of about 1 million stars in 10^m-19^m magnitude range within 255 selected areas of northern sky. The XC1 catalogue is based on our results of measurements and astrometric reduction of digitized images of Schmidt plates POSS-I and POSS-II sky surveys, obtained from USNOFS PMM Image Archive. The Tycho-2 catalogue was used as reference one. The

epoch difference between these surveys is about 45 years. Here is present only 255 selected fields from XC1 catalogue. In these 255 selected fields minimum 5 individual positions from O, E, J, F, and N plates were used to derive mean positions and proper motions. Additionally, the 2MASS positions for identified stars also were used. For the rest about of 100 fields, the quality of some images is unsatisfactory, so we were not able to use all 5 individual positions to derive mean positions and proper motions.

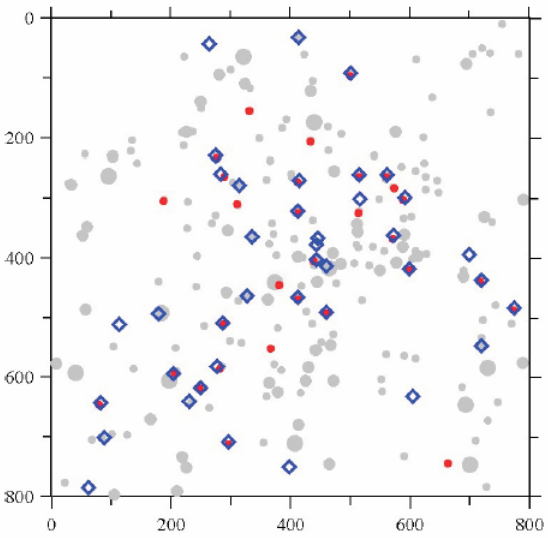

Figure 38. The finding chart for the variable stars in the central region of the globular cluster M15. The size and orientation of the plot corresponds to orientation of WFPC1 chip of HST during M15 observations (≈35″ 35 ″, cf. Fig. 37), the axes designation is given in units of WFPC1 pixels. The variables discovered with the HST and with 4.2-m WH telescope are plotted as red dots, the variables from our list are plotted as blue open diamonds. Black open circles denote brightest non-variable stars measured with HST in M15; the circle size roughly proportional to star's R magnitude

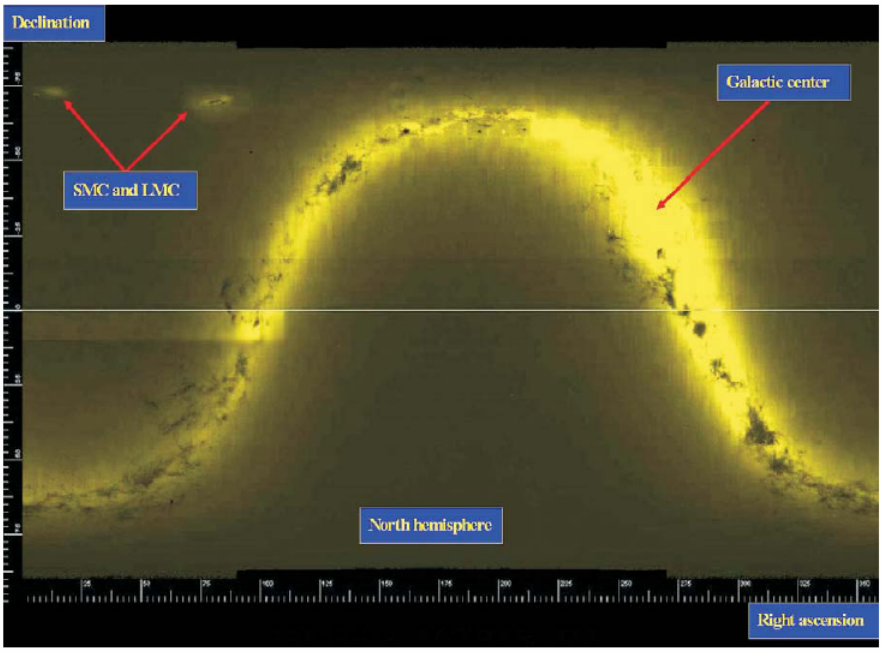

Figure 39. The distribution of the XPM catalogue stars

The averaged internal errors of the positions (on J2000) are about 70 to 100 mas for stars < 17^m-18^m and are 100 to 200 mas for faintest stars. Proper motions are derived from comparison POSS-1 and POSS-2 epoch positions. Their internal errors are about 2 to 5 mas/y, depending on magnitude. In order to estimate external errors of the XC1 catalogue, various external comparisons with modern catalogues were performed. The significant systematic errors in XC1 positions and proper motions have not been found. The estimated external proper motion errors for stars fainter than 15^m are 3÷5 mas/yr, depending on magnitude. Magnitude-depended systematic errors were removed. Color-depended systematic errors were not removed.

Catalogue	UCAC2	2MASS	CMC14	KMAC1CU	DR3	LEDA
Number of common stars	118786	551641	355111	34869	285	4195
Percent of the stars with position deviations more 3σ	4 %	3.5 %	3.5 %	3.5 %	1.5 %	2.5 %
The RMS errors of position differences, mas	50–150	70–350	70–250	80–600	110	600
Systematic differences in RA, mas	-10..+10 ±2	-10..+10 ±1.5	-20..+10 ±2	-50..+20 ±5	+12 ±6	-460 ±9
Systematic differences in DEC, mas	-10..+10 ±2	-10..+10 ±1.5	0...+40 ±2	-20..0 ±5	-2 ±7	-89 ±9
The RMS errors of proper motion differences, mas/yr	2.5–6	–	–	–	3.3	4.0
Systematic differences in proper motion by RA, mas/yr	-1..+1 ±0.1	–	–	–	-0.18 ±0.2	+0.07 ±0.06
Systematic differences in proper motion by DEC, mas/yr	-1..+1 ±0.1	–	–	–	-0.12 ±0.2	+0.24 ±0.06

The XC1 catalogue is available: *http://cdsweb.u-strasbg.fr/cgi-bin/qcat?I/302*

4.11. Absolute proper motions of 280 millions stars from 2MASS and USNOA2.0 data

P. Fedorov, A. Myznikov, V. Akhmetov

We combined the data from 2MASS and dUSNO-A2.0 catalogues in order to derive absolute proper motions of about 280 millions stars fainter than 12^m, covering the all sky excluding a narrow zone along the galactic equator. The proper motions were derived from 2MASS Point Sources Catalog and USNO-A2.0 positions with mean epoch difference about of 45 years for northern hemisphere and about of 17 years for south. The absolutization was done using about 1.4 million galaxies from 2MASS Extended Sources

Catalog. Before deriving the proper motions, the most of intrinsic to USNO-A2.0 zonal systematic errors were corrected. Mean formal error of absolutization is less than 1 mas/yr. The catalog named XPM contains the ICRS positions of stars at the J2000 epoch, original absolute proper motions, as well as B, R, J, H, and Ks magnitudes.

The cross-identification, error correction, linking to extragalactic objects and deriving the proper motions were done for individual USNO-A2.0 fields. Each field has a size about of 5x5 degrees and has a constant value of epoch of observation. Because of very big difference of star density at different galactic latitudes, we used 2-step cross-identification procedure with circular window of adjustable size. This algorithm cannot guarantee right identification for all objects, but we believe that overwhelming majority of objects was identified correctly. Thus, the maximal value of proper motion varies from about 80 mas/yr in dense fields up to 350 mas/yr in low-density fields. After the cross-identification the 2MASS minus USNO-A2.0 coordinate differences for identified stars were analyzed inside each field in order to find out possible geometric distortions induced by both USNO-A2.0 and 2MASS systematic errors.

Systematic coordinate differences were approximated inside each field by a combination of low-power polynomial and high-frequency stepping function. Since we do not know which exactly part of systematic differences is introduced by real motion of the stars, we made corrections for coordinates of all USNO-A2.0 objects, with no distinct the stars and galaxies, and just reduced USNO-A2.0 into the coordinate system defined by 2MASS stars in the particular field, getting zero mean systematic differences between 2MASS and USNO-A2.0 stars. In order to get the reference to extragalactic objects, we search for 2MASS extended sources among USNO-A2.0 objects inside each field. The number *N* of identified extragalactic objects inside a field varies from a few tens at low galactic latitudes up to several thousands at high galactic latitudes. Because the most of extended sources are galaxies, the differences between their 2MASS and USNO-A2.0 coordinates at this stage just reflect the real star motions with opposite sign (postulating zero proper motion for galaxies).These differences inside each field were approximated by a simple linear reduction model and used for reduction whole USNO-A2.0 into coordinate system defined by 2MASS extended sources. The root-mean-squared deviation of differences is about 400-450 mas, so we expect the error of absolutization to be roughly $\varepsilon = \sigma / (\sqrt{N}\Delta T)$ = 0.2 … 3 mas/yr at the North, and 3 times larger at the South. The proper motions of stars were derived at the final stage by dividing the coordinate difference by epoch difference for the each star. In order to estimate external errors of the proper

motions derived, we identified about of 12000 quasars from DR5 and LEDA data sets among our stars, and analyzed their formal proper motions. As was expected, we see zero mean value of the formal proper motions and root-mean-squared value to be 3-8 mas/yr depending on magnitude. Figure 39 shows the distribution of stars from the catalogue XPM, which will be used for determination of kinematic characteristics of our Galaxy.

Today there is no a big full-sky catalogues of absolute proper motions for the faint stars, though there are many tasks where they are applicable. In this work we do not corrected the proper motions derived for the magnitude equation, but we believe that it should be negligible in faint magnitude range. The magnitude equation is seems to be considerable for stars brighter than 15^m. This fact hampers the comparisons of the proper motions of faint stars with those from most of modern catalogues, such as UCAC-2 and Tycho-2. Additionally we have suspicion that measured coordinates of extended objects can be shifted relative to measured coordinates of stars in 2MASS and USNO-A2.0 catalogues. This effect can be hard to detect and measure, but it can lead to problems with agreement of zero-points for different catalogues, referenced to extragalactic objects. At the moment we do detailed analysis of results obtained, as well as do the kinematics analysis of the catalogue.

5. Other activities

Teaching

The following selected special courses were proposed for astronomy students:

1. Dr. Fedorov P. N. Fundamental astrometry: new approaches
2. Prof. Alexandrov Yu. V. Introduction to astronautic, Problems of modern astrophysics
3. Dr. Gretsky A. M. New methods in astrophysics
4. Dr. Stankevich D. G. Astronomical image processing
5. Dr. Gretsky A. M. Infrared astronomy
6. Dr. Zakhozhay V. A. Structure and evolution of the galaxy
7. Prof. Shkuratov Yu. G. Optics of planetary surface

Selected Co-operation

1. Institute of Radio Astronomy of National Academy of Sciences of Ukraine: Ukrainian lunar satellite project (Yu. G. Shkuratov), gravitational lensing (V. N. Dudinov,

V. G. Vakulik, A.P. Zheleznyak), radar and photometric observations of NEAs (D.F. Lupishko, F. P. Velichko, V. G. Shevchenko, Yu. N. Krugly).

2. Main Astronomical Observatory of National Academy of Sciences of Ukraine: Space spectropolarimeter for International Space Station (V. V. Korokhin, V. V. Konichek, V. A. Psarev), astrometry (P. N. Fedorov).
3. Crimean Astrophysical Observatory: Solar physics researches (L. A. Akimov, I. L. Belkina, V. V. Korokhin), observations of asteroids and comets (D. F. Lupishko, N. N. Kiselev, V. G. Shevchenko, Yu. N. Krugly, I. N. Belskaya), observation of the Moon (N. V. Opanasenko).
4. Astronomical Observatory of Kiev National University: Asteroid defense (D. F. Lupishko), cometary observations (V. S. Filonenko).
5. Institute for Radiophysics and electronics of National Academy of Sciences of Ukraine: New automatic spectroheliograph for solar researching and monitoring programs (L. A. Akimov, V. V. Korokhin, V. V. Konichek, I. E. Sinelnikov).
6. Institute of Space Researches, Russia: “Coronas-F” data processing and analysis (L. A. Akimov, I. L. Belkina, V. V. Korokhin).
7. V. I. Vernadsky Instutute of Geochemistry and Analytical Chemistry: Joint studies of the Moon, Mars, and Venus (Yu. G. Shkuartov).
8. Ulugh Beg Astronomical Institute of Academy of Sciences of Uzbekistan: Gravitational lensing (V. N. Dudinov, V. G. Vakulik, A. P. Zheleznyak).
9. Brown University (USA): Joint studies of the Moon, Mars, and Venus (Yu. G. Shkuartov, D. G. Stankevich).
10. Army Research Laboratory (USA): DDA modeling light scattering by particles with various shapes (Yu. G. Shkuratov, D. V. Petrov, E. S. Zubko).
11. Naval Research Laboratory (USA): DDA modeling light scattering by particles with various shapes (Yu. G. Shkuratov, D. V. Petrov, E. S. Zubko, A. A. Ovcharenko, S. Yu. Bondarenko).
12. JPL NASA (USA): Joint measurements of structure analogs of planetary regoliths (A. A. Ovcharenko, Yu. G. Shkuratov).
13. Cornell University (USA): Studies of fractal-like surfaces (Yu. G. Shkuratov).
14. World Data Center WDC Boulder Co, (USA): Solar activity service (L. A. Akimov, I. L. Belkina, V. V. Korokhin).
15. Harvard-Smithsonian Center for Astrophysics (USA): Gravitational lensing (V. N. Dudinov, V. G. Vakulik, A. P. Zheleznyak).

16. Astronomical Observatory of Helsinki University (Finland): Light scattering problems (Yu. G. Shkuratov, A. A. Ovcharenko, and D. G. Stankevich).
17. Oulu University (Finland): Venus geological studies (V. G. Kaydash).
18. Max Plank Institute fur Aeronomy, Katlenburg-Lindau, Germany: Lunar space missions (V. V. Korokhin, V. G. Kaydash, Yu. G. Shkuratov).
19. DLR, Berlin (Germany): Organic matter in the space (L. V. Starukhina).
20. Observatoire de Paris, Meudon, France: Studies of Kuiper Belt Objects (I. N. Belskaya).
21. Observatoire Midi Perinees, Toulouse, France: Studies of light scattering by terrestrial samples and computer ray-tracing in models of particulate surfaces (Yu. G. Shkuratov, D. G. Stankevich, A. A. Ovcharenko).
22. Torino Osservatorio, Italy: Study of asteroids (I. N. Belskaya, D. F. Lupishko).
23. Poznan' Astronomical Observatory of Adam Mickievicz University, Poland: Joint observations (F. P. Velichko, V. G. Shevchenko).
24. Astronomical Institute of the Czech Republic Academy of Sciences: Photometry of near-Earth asteroids (Yu. N. Krugly).

6. Selected papers

(In case of joint papers we mark the authors from our Institute)

1. Akimov L.A Light reflection by the Moon.I // Kinematika i Fizika Nebesnykh Tel. – 1988. – 4, no. 1. – 3-10. [in Russian]

2. Akimov L.A. Light reflection by the Moon.II // Kinematika i Fizika Nebesnykh Tel. – 1988. – 4, no. 2. – 10-16. [in Russian]

3. Akimov L.A., Beletskiy S.A., Belkina I.L., Bugaenko O.I., Velikodskiy Yu.I., Zhitnik, I.A., Ignat'ev A.P., Korokhin V.V., Kuzin S.V., Marchenko G.P., Pertsov A.A. Quasi-Periodicity of MgXII X-ray Bursts Revealed by CORONAS-F SPIRIT Data for Solar Active Regions // Astronomy Reports. – 2005. – 49, Issue 7. – 579-586.

4. Akimov L.A., Bogovskiy V.K., Grigorenco E.I., Taran V.I., Chernogor L.F. Atmospheric-Ionospheric effects of the solar eclipse of May 31, 2003, in Kharkov // Geomagnetism and Aeronomy. – 2005. – 45, N 4. – 526-551.

5. Alexandrov Yu.V. Physics of Planets, Kharkiv Univ. – 1996. – 423 p. [in Ukrainian]

6. Alexandrov Yu.V. Celestial Mechanics, Kharkiv Univ. – 2006. – 227 p. [in Ukrainian]

7. Alexandrov Yu.V. Multidimentional Cosmology, Kharkiv Univ. – 2007. – 56 p.

8. Belskaya I.N., Shevchenko V.G. 2000. Opposition effect of asteroids // Icarus – 147. – 94-105.

9. Belskaya I.N., Shkuratov Yu.G., Efimov Yu.S., Shakhovskoy N.M., Gil-Hutton R., Cellino A., Zubko E.S., Ovcharenko A.A., Bondarenko S.Yu., Shevchenko V.G., Fornasier S., Barbieri C. The F-type asteroids with small inversion angles of polarization // Icarus – 2005. – 178. – 213-221.

10. Belskaya I.N., Ortiz J.L., Rousselot P., Ivanova V., Borisov G., Shevchenko V.G., Peixinho N. Low phase angle effects in photometry of trans-neptunian objects: 20000 Varuna and 1996 TO66 // Icarus – 2006. – 184. – 277-284.

11. Belskaya I.N., Levasseur-Regourd A.-C., Shkuratov Yu.G., Muinonen K. Surface properties of Kuiper-Belt objects and Centaurs from photometry and polarimetry // In: The Solar System Beyound Neptune (Barucci, A., et al., Eds.), University of Arizona Press, Tucson, Arizona, USA., - 2008. - 115-127.

12. Chiorny V.G., Shevchenko V.G., Krugly Yu.N., Velichko F.P., Gaftonyuk N.M. Photometry of asteroids: Lightcurves of 24 asteroids obtained in 1993-2005 // Planet. Space Sci. – 2007. – 55. – 986-997.

13. Dudinov V.N., Vakulik V.G., Zheleznyak A.P., Konichek V.V., Tsvetkova V.S., Chodzhayev A.S. Observations of Jupiter from Central Asia during the SL-9 crash. // In: ESO Conference and Workshop Proceedings No.52, Febr. – 1995, R.West and H.Bohnhardt Eds., pp. 323-326.

14. Dudinov V.N., Konichek V.V., Kuz'menkov S.G., et al. Speckle interferometry with the BTA telescope. // In: "Instrumentation for Astronomy with Large Optical Telescopes", Colloq. No.67 IAU Commission No. 9, 1982, pp. 191-198.

15. Dudinov V.N., Tsvetkova V.S., Novikov S.B., Pronik I.I. Signs of interaction of the NGC1275 nucleus with the high-velocity system according to 0.7-arcsec seeing observations. In:"Paired and Interacting Galaxies", IAU Coll. No.124, Dec.1989, Univ. Alabama at Tuscaloose, 1990. –pp. 421-429.

16. Fedorov P.N., Myznikov A.A. The X1 catalogue of positions and proper motions of faint stars around the ICRF sources // Kinematika i Fizika Nebesnykh Tel, Suppl. – 2005. – 5. – 322-327.

17. Fedorov P.N., Myznikov A.A. XC1 catalogue of positions and proper motions (Fedorov+, 2005) // VizieR On-line Data Catalog: http://cdsweb.u-strasbg.fr/viz-bin/qcat?XC1.

18. Filonenko V.S., Churyumov K.I. New peculiarities of cometary outburst Activity // Advances in Space Res. – 2006. – 38. – 1940-1945.

19. Filonenko V.S., Churyumov K.I. An investigation of the light curve of deep impact target comet // Advances in Geosci. – 2006. – 3. – 185-189.

20. Korokhin V.V., Velikodsky Yu.I., Shkuratov Yu.G., Mall U. The Phase Dependence of Brightness and Color of the Lunar Surface: a Study Based on Integral Photometric Data // Solar System Res. – 2007. – 41, No.1. – 19-27.

21. Korokhin V. V., Kaydash V. G., Shkuratov Yu. G., Stankevich D. G., Mall U. Prognosis of TiO_2 abundance in lunar soil using a non-linear analysis of Clementine and LSCC data // Planet. Space Sci. -2008. -56. -1063–1078.

22. Krugly Yu.N. Problems of CCD photometry of fast-moving asteroids // Solar System Res. – 2004. – 38**,** № 3. – 241-248.

23. Krugly Yu.N., Maccone C., Gaftonyuk N.M., Lupishko D.F., Shevchenko V.G., Velichko F.P. 11264 Claudiomaccone: Binary small main-belt asteroid // Planet. Space Sci. – 2007. – 55, Issue 4. – 449-454.

24. Lupishko D.F., Belskaya I.N. On the surface composition of the M-type asteroids // Icarus – 1989. – 78. – 395-401.

25. Lupishko D.F., Vasilyev S.V., Efimov Yu.S., Shakhovskoj N.M. UBVRI-polarimetry of asteroid 4179 Toutatis // Icarus – 1995. – 113. – 200-205.

26. Lupishko D.F., Di Martino M., Binzel R.P. Near-Earth objects as principal impactors of the Earth: Physical properties and sources of origin // In: “Near Earth Objects, our Celestial Neighbors: Opportu-nity and Risk”, Proc. of IAU Symp. 236. (Eds. A. Milani et al) Cambridge Univ. Press, - 2007. – 251-260.

27. Petrov D., Shkuratov Yu., Videen G. The influence of corrugation on light-scattering properties of capsule and finite cylinder particles: *Sh*-matrices analysis // Journ. Quant. Spectrosc. Rad. Transfer – 2008. – 109. – 650–669.

28. Petrov D., Shkuratov Yu., Videen G. Analytic light-scattering solution of two merging spheres using Sh-matrices // Optics Communications -2008. -281. -2411–2423.

29. Pieters C., Shkuratov Yu., Kaydash V., Stankevich D., Taylor L. Lunar soil characterization consortium analyses: pyroxene and maturity estimates derived from Clementine image data // Icarus – 2006. – 184. – 83-101.

30. Pluzhnik, E. A. Differential photometry of speckle-interferometric binary and multiple stars // Astron. Astrophys. – 2005. – 431. – 587-596.

31. Psarev V., Ovcharenko A., Shkuratov Yu., Belskaya I., Videen G. Photometry of surfaces with complicated structure at extremely small phase angles // Journ. Quant. Spectrosc. Rad. Transfer – 2007. – 106. – 455–463.

32. Schild R., Vakulik V. Microlensing of a Ring Model for Quasar Structure // Astron. J. – 2003. – 126, №2. – 689-695.

33. Shalygina, O.S., Korokhin, V.V., Starukhina, L.V., Shalygin, E.V., Marchenko, G.P., Velikodsky, Yu. I., Starodubtseva, O. M., Akimov, L. A. The north-south asymmetry of polarization of Jupiter: The causes of seasonal variations // Solar System Res. – 2008. – 42, Issue 1. – 8-17.

34. Shevchenko V.G., Tedesco E.F. 2006. Asteroid albedos deduced from stellar occultations. Icarus. 184, 211-220.

35. Shkuratov Y. G., Starukhina L. V., Hoffmann H., Arnold G. A model of spectral albedo of particulate surfaces: Implications for optical properties of the Moon // Icarus – 1999. – 137. – 235-246.

36. Shkuratov Yu. G., Lytvynenko L. M., Shulga V. M., Yatskiv Ya. S., Vidmachenko A. P., Kislyuk V. S. Objectives of a prospective Ukrainian orbiter mission to the moon // Adv. Space Res. – 2003. – 31, No. 11. – 2341-2345.

37. Shkuratov Yu.G., Petrov D.V., Videen G. Classical photometry of pre-fractal surfaces // J. Opt. Soc. Am. – 2003. – 20, No. 11. – 2081-2092.

38. Shkuratov Yu., Kreslavsky M., Kaydash V., Videen G., Bell III J., Wolff M., Hubbard M., Noll K., Lubenow A. Hubble space telescope imaging polarimetry of Mars during the 2003 opposition // Icarus – 2005. – 176. – 1-11.

39. Shkuratov Yu., Bondarenko S., Kaydash V., Videen G., Muños O., Volten H. Photometry and polarimetry of particulate surfaces and aerosol particles over a wide range of phase angles // Journ. Quant. Spectrosc. Rad. Transfer – 2007. – 106. – 487–508.

40. Starodubtseva O.M., Akimov L.A., Korokhin V.V. Temporal changes in the North-South asymmetry of polarized light of Jupiter may be associated with the Comet SL9 visit to the Jovian system // Planet. Space Sci. – 1997. – 45, N 10. – 1183-1188.

41. Starodubtseva O.M., Akimov L.A., Korokhin V.V. Seasonal variation of the North-South asymmetry of polarized light of Jupiter // Icarus – 2002. – 157, No2. – 419-425.

42. Starukhina L. V. Light absorption by radiation-induced hydroxyl ions and the problem of finding water on atmosphereless celestial bodies // Solar System Res. 1999. – 33, No.4. – 291-295.

43. Starukhina L. V. On the origin of excess hydrogen at the lunar poles // Solar System Res. – 2000. – 34, No. 3. – 215-219.

44. Starukhina L. V. Water detection on atmosphereless celestial bodies: Alternative explanations of the observations. J. Geophys. Res. Planets – 2001. – 106, No E7. – 14701-14710.

45. Starukhina L. V., and Shkuratov Yu. G. The lunar poles: water ice or chemically trapped hydrogen? // Icarus – 2000. – 147, No 2. – 585-587.

46. Tsvetkova V.S., Dudinov V.N., Novikov S.B., et al. Shape and size of asteroid 4 Vesta: speckle interferometry and polarimetry // Icarus – 1991. – 92. – 342-349.

47. Vakulik V.G., Schild R.E., Smirnov G.V., et al. Q2237+0305 source structure and dimensions from light curves simulation // Month. Not. Roy. Astron. Soc. – 2007. – 382. – 819-826.

48. Velichko S., Kiselev N., Velichko F. Polarimetry and Photometry of Comet C/2004 Q2 (Machholz) // Earth, Moon, and Planets. – 2006. – 97. – 379-386.

49. Zubko E., Muinonen K., Shkuratov Yu., Videen G., Nousiainen T. Scattering of light by roughened Gaussian random particles // Journ. Quant. Spectroscopy Radiative Transfer – 2007. – 106. – 604–615.

50. Zubko E., Shkuratov Y., Mishchenko M., Videen G. Light scattering in a finite multi-particle system // Jorn. Quant. Spectrosc. Rad. Transfer -2008. -109. -2195–2206.